Available online at www.sciencedirect.com
SCIENCE DIRECT®
International Journal of Solids and Structures 42 (2005) 1613–1647
INTERNATIONAL JOURNAL OF SOLIDS and STRUCTURES
www.elsevier.com/locate/ijsolstr

Evanescent and propagating waves in prestretched hyperelastic plates ☆

Baruch Karp [a,*], David Durban [b]

[a] Department of Mechanical Engineering, Ben-Gurion University of the Negev, P.O.B. 653, Beer-Sheva 84105, Israel
[b] Faculty of Aerospace Engineering, Technion—Israel Institute of Technology, Haifa 32000, Israel

Received 14 February 2004; received in revised form 28 July 2004
Available online 18 September 2004

Abstract

A detailed spectral analysis is presented for dynamic eigenfields generated by time harmonic edge perturbations applied to a semi-infinite prestrained plate. Formulation is exact within continuum elasticity theory and frequency maps are provided over a range of prestrain, material (hyperelastic) properties, boundary conditions and frequency of applied disturbance.

We concentrate mainly on numerical findings for the complex wave numbers associated with evanescent waves. Asymptotic expansions, at the limit of low frequency and near cut-off frequencies are given. An appreciable depth of penetration of evanescent waves is found to characterize frequencies just below any cut-off frequency. Cut-off frequencies, independent of boundary conditions, are highly sensitive to material properties and their explicit dependence on prestrain level has been exposed. Asymptotic solutions of the frequency equations, for the propagating modes in the long wavelength region, are added to enhance and to support the numerical results. The influence of symmetric boundary conditions over the long faces (free, clamped, sliding and inextensional) on the wave behaviour is highlighted. Application of the results to non-symmetric boundary conditions is suggested.

Keywords: Wave propagation; Evanescent waves; End effects; Plates; Hyperelastic solids

1. Introduction

Existing studies on steady state wave behaviour of prestrained plates concentrate almost exclusively on propagating modes with just a limited number of studies devoted to the evanescent waves.

☆ This work is based in part on a D.Sc. Thesis submitted to the Technion.

* Corresponding author. Tel.: +972 86410694; fax: +972 86431291.
E-mail address: bkarp@bgumail.bgu.ac.il (B. Karp).

0020-7683/$ - see front matter © 2004 Elsevier Ltd. All rights reserved.
doi:10.1016/j.ijsolstr.2004.07.029

Propagating modes are relevant to wave-propagation, vibration and quasi-static stability examinations and are discussed extensively for prestrained waveguides (e.g. Ogden and Roxburgh, 1993 for hyperelastic waveguide; Rogerson and Cai, 2000 for fiber-reinforced layer). The evanescent modes, on the other hand, are energy trapping and related to the construction of a possible dynamic version of Saint-Venant's principle (Torvik, 1967; Karp and Durban, 1997). These waves also have a contribution to dynamical stress concentration (McCoy, 1968). The quasi-static counterpart of evanescent waves, elastic eigenfunctions, are extensively explored in the context of end effects (Horgan and Knowles, 1983) and commonly accepted as providing an estimate for the validity of Saint-Venant's principle in elastostatics.

Here, we present a detailed study of both propagating and evanescent modes that develop in a prestrained plate (Karp, 1996) with emphasis on the latter. The setting is similar to that of the quasistatic analysis in (Karp and Durban, 2002). A hyperelastic semi-infinite plate is uniformly stretched, under plane strain conditions, in the axial direction. A time harmonic incremental perturbation is then applied at the end. We analyze the spectrum of the eigenmodes, both propagating and evanescent, that will potentially contribute to the actual response of the plate.

The mathematical formulation is within the framework of continuum elasticity, accounting for large deformations, with various boundary conditions imposed over the long faces of the plate. A separation of variables solution is assumed with due distinction between symmetric and antisymmetric eigenmodes. Our main interest is in the sensitivity of the modes to the level of prestrain, boundary conditions over the long faces, constitutive parameters and the frequency of applied disturbance.

Compliance with boundary data generates transcendental equations for the wavenumbers at a given frequency, initial stretch, material properties and boundary conditions. Four sets of boundary conditions have been examined which include free, clamped, sliding and inextentional boundaries. Material behaviour is modeled by hyperelastic strain energy functions for three different materials (with experimentally determined coefficients), over a wide range of initial stretch.

Frequency maps are displayed in some detail to assess the various sensitivities of the wavenumber for evanescent waves to prestrain, boundary conditions, material properties and frequency. It has been found that the eigensolutions for symmetric boundary conditions can be used, with appropriate adjustments, to represent wave behaviour in waveguides with non-symmetric boundary conditions.

We have studied the influence of initial stretch λ and exciting frequency Ω, for three material models and four sets of ideal boundary conditions, with the main results supported by asymptotic expansions. The imaginary part of the smallest complex eigenvalue, inversely related to depth of penetration, is examined in particular and illustrated over a range of parameters. High sensitivity of that eigenvalue is exposed, especially, near cut-off frequencies. Due to this importance of cut-off frequencies, their explicit dependence on the prestretch is derived.

It was found that plates with free faces and plates with clamped faces share similar frequency maps, both qualitatively and quantitatively (except for the fundamental modes). Plates with sliding and inextensional faces share the same frequency maps (again with the exception of fundamental modes).

Asymptotical expansions near several limiting points (cut-off frequencies, quasi-static response, long wave length limit and bifurcation points) are given and used to assess the numerical results.

2. Time harmonic response of a prestrained plate

A uniformly strained semi-infinite plate (Fig. 1) is characterized by the principal stretches λ_x, $\lambda_y \equiv 1$ and $\lambda_z \equiv \lambda$. Plane-strain conditions are assumed under uniform axial tension stress $\sigma_z = \sigma$. The origin of the Cartesian system (x, y, z) is located at the center of the free $z = 0$, along with the associated unit triad $(\boldsymbol{i}, \boldsymbol{j}, \boldsymbol{k})$, where the deformed thickness is denoted by $2h$.

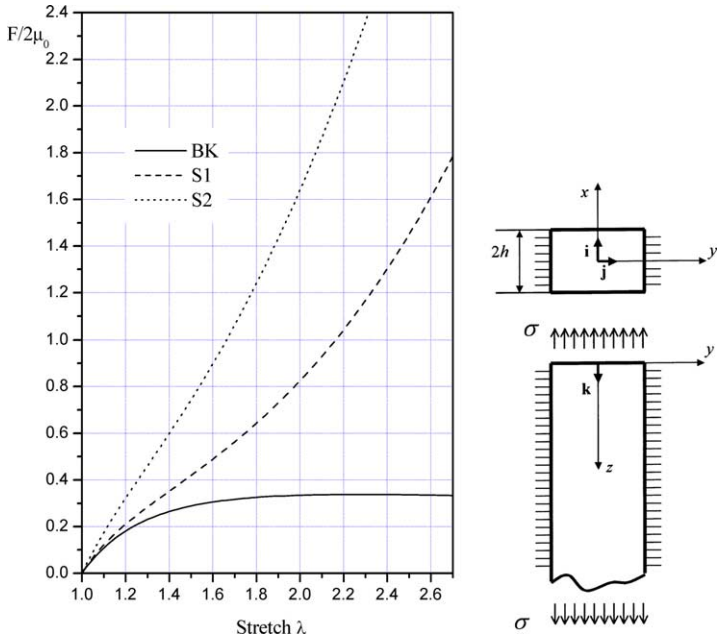

Fig. 1. A semi-infinite ($z \geqslant 0$) plate under uniform stress σ. Plane strain conditions are imposed in the y-direction and current thickness is $2h$. Also shown are the plane-strain curves of force-stretch for the three hyperelastic materials considered in the paper (A.5)–(A.7).

Assume now a time harmonic incremental end disturbance, applied over the end of the plate, which induces the perturbed velocity

$$\mathbf{V} = u\boldsymbol{i} + w\boldsymbol{k} \tag{2.1}$$

within the plate. Restricting the discussion to plane-strain response, we find that both velocity components (u, w) depend only on x and z. The Eulerian strain rate components are therefore

$$\varepsilon_x = u_{,x}, \quad \gamma_{xz} = 1/2(u_{,z} + w_{,x}), \quad \varepsilon_z = w_{,z}. \tag{2.2}$$

Incremental plane-strain response is described in the form, suggested by Hill (1979),

$$\overset{\nabla}{\sigma}_x = a\varepsilon_x + c\varepsilon_z, \quad \overset{\nabla}{\tau}_{xz} = 2\mu\gamma_{xy}, \quad \overset{\nabla}{\sigma}_z = (c - \sigma)\varepsilon_x + b\varepsilon_z \tag{2.3}$$

where $\left(\overset{\nabla}{\sigma}_x, \overset{\nabla}{\tau}_{xz}, \overset{\nabla}{\sigma}_z\right)$ are the objective Jaumann stress rates and $(a, b, c, 2\mu)$ denote instantaneous material moduli. Relations (2.3) cover a wide family of solids including hyperelastic materials (Appendix A) for which these moduli depend on the prestrain λ.

The rate form of the two equations of motion (Karp, 1996) for the uniformly strained plate is given by

$$au_{,xx} + \beta u_{,zz} + (c + \alpha)w_{,xz} = \rho u_{,tt} \tag{2.4}$$

$$(c + \alpha)u_{,xz} + \alpha w_{,xx} + bw_{,zz} = \rho w_{,tt} \tag{2.5}$$

with

$$\alpha = \mu - \frac{1}{2}\sigma, \quad \beta = \mu + \frac{1}{2}\sigma \tag{2.6}$$

where ρ is the mass density at the homogeneous prestrained state, and t denote the time. In the absence of the inertia terms we recover from (2.4) and (2.5) the quasistatic rate equilibrium equations of Hill (1979).

Reference phase velocities of transverse waves (C_{T}) and longitudinal waves (C_{L}) follow from (2.4) and (2.5) as

$$C_{\mathrm{T}x}^2 = \frac{\alpha}{\rho}, \quad C_{\mathrm{T}z}^2 = \frac{\beta}{\rho}, \quad C_{\mathrm{L}x}^2 = \frac{a}{\rho}, \quad C_{\mathrm{L}z}^2 = \frac{b}{\rho} \tag{2.7}$$

where the indices (x,z) denote the direction of wave propagation.

Along the faces $x = \pm h$ we impose boundary conditions which require various combinations of vanishing velocity components in (2.1) and traction rate vector components given by (Karp and Durban, 2002)

$$\pm\mathbf{t}_x = \overset{\nabla}{\sigma}_x\mathbf{i} + \left(\overset{\nabla}{\tau}_{xz} - \sigma\gamma_{xy}\right)\mathbf{k} \quad \text{at } x = \pm h \tag{2.8}$$

Using the kinematic relations (2.2) and the constitutive equations (2.3) it is possible to express the boundary data in terms of velocity components for four ideal and symmetric cases:

For free boundaries (FR) where $\boldsymbol{t}_x$ vanishes we have

$$au_{,x} + cw_{,z} = 0, \quad u_{,z} + w_{,x} = 0 \qquad \text{at } x = \pm h \tag{2.9}$$

For clamped boundaries (CL) where $\mathbf{V}$ vanishes we find

$$u = 0, \quad w = 0 \qquad \text{at } x = \pm h \tag{2.10}$$

For sliding (frictionless) boundaries (SL), both shear traction rate and normal velocity have to vanish

$$u = 0, \quad u_{,z} + w_{,x} = 0 \qquad \text{at } x = \pm h \tag{2.11}$$

Finally, for inextensional boundaries (IN), there is no sliding and no normal traction rate

$$au_{,x} + cw_{,z} = 0, \quad w = 0 \qquad \text{at } x = \pm h \tag{2.12}$$

Notice that these boundary conditions are imposed simultaneously with the application of the end disturbance.

Time harmonic eigenfields of Eqs. (2.4) and (2.5), compatible with any of the boundary conditions (2.9)–(2.12), are now sought in the usual separation-of-variables solution space

$$u = U(x)\exp\left(\frac{\mathrm{i}\pi kz}{2h} - \mathrm{i}\omega t\right), \quad w = W(x)\exp\left(\frac{\mathrm{i}\pi kz}{2h} - \mathrm{i}\omega t\right) \tag{2.13}$$

where $U(x)$ and $W(x)$ are transverse velocity profiles, k is the associated non-dimensional wave number and ω is the circular frequency. Substituting (2.13) in the differential equations (2.4) and (2.5) and noting the symmetry of all boundary data, we can separate the solution into symmetric patterns

$$U_s = A_1\sinh\left(\Gamma_1\frac{\pi kx}{2h}\right) + A_2\sinh\left(\Gamma_2\frac{\pi kx}{2h}\right) \tag{2.14a}$$

$$W_s = A_1\eta_1\cosh\left(\Gamma_1\frac{\pi kx}{2h}\right) + A_2\eta_2\cosh\left(\Gamma_2\frac{\pi kx}{2h}\right) \tag{2.14b}$$

and antisymmetric patterns

$$U_a = A_3\cosh\left(\Gamma_1\frac{\pi kx}{2h}\right) + A_4\cosh\left(\Gamma_2\frac{\pi kx}{2h}\right) \tag{2.15a}$$

$$W_a = A_3\eta_1 \sinh\left(\Gamma_1 \frac{\pi k x}{2h}\right) + A_4\eta_2 \sinh\left(\Gamma_2 \frac{\pi k x}{2h}\right) \tag{2.15b}$$

Here A_1–A_4 are integration constants,

$$\eta_p = \frac{i\left(a\Gamma_p^2 - \bar{\beta}\right)}{\Gamma_p(c+\alpha)} \quad p = 1,2 \tag{2.16}$$

and (Γ_1, Γ_2) are the roots of the characteristic equation of (2.4) and (2.5)

$$a\alpha\Gamma^4 - \bar{d}\Gamma^2 + \bar{b}\bar{\beta} = 0 \tag{2.17}$$

where

$$\bar{b} \equiv b - \beta C^2, \quad \bar{\beta} \equiv \beta(1 - C^2) \tag{2.18}$$

with C denoting the non-dimensional phase velocity

$$C \equiv \frac{\Omega}{k} \quad \text{with } \Omega \equiv \frac{2h\omega}{\pi C_{T_z}} \tag{2.19}$$

The roots (Γ_1, Γ_2) of (2.17) are given explicitly by

$$\Gamma_1 = \sqrt{\frac{\bar{d} - \sqrt{\bar{d}^2 - 4a\bar{b}\alpha\bar{\beta}}}{2a\alpha}}, \quad \Gamma_2 = \sqrt{\frac{\bar{d} + \sqrt{\bar{d}^2 - 4a\bar{b}\alpha\bar{\beta}}}{2a\alpha}} \tag{2.20}$$

where

$$\bar{d} \equiv a\bar{b} + \alpha\bar{\beta} - (c+\alpha)^2 = d - \beta(a+\alpha)C^2 \tag{2.21}$$

and

$$d \equiv ab + \alpha\beta - (c+\alpha)^2 \tag{2.22}$$

Imposing the boundary conditions (2.9)–(2.12) on the velocity profiles (2.13) generates in each case transcendental equations for the wave number k at a given frequency ω. A detailed mapping of the wave numbers for three different material models is given in the next section. Values of the wave number appear in pairs of opposite sign ($\pm k$) or as complex conjugates and depend on frequency Ω, boundary data, initial stretch λ and material properties. For propagating waves, k is purely real and will be labeled as "*wave constant*". For purely imaginary values of the wave number we shall consider only the evanescent fields, where $ik < 0$, labeling the positive value of $\mathrm{Im}\{k\}$ as "*attenuation constant*". That term will be also used for labeling the positive imaginary part of complex wave numbers. Thus, with the notation $k = J + iK$, where both J, K are real, we consider eigenvalues where $K \geqslant 0$. Propagating waves are identified with $K = 0$ with J then denoting the wave constant. For imaginary or complex values of the wave number k, the smallest (positive) value of the attenuation constant K provides an upper bound on the depth of penetration of evanescent waves.

The boundary conditions (2.9)–(2.12) are conveniently restated in terms of the velocity profiles as follows:

Free boundaries (FR):

$$aU' + \left(\frac{i\pi k}{2h}\right)cW = 0, \quad \left(\frac{i\pi k}{2h}\right)U + W' = 0 \qquad \text{at } x = \pm h \tag{2.23}$$

Clamped boundaries (CL):

$$U = 0, \quad W = 0 \qquad \text{at } x = \pm h \tag{2.24}$$

Sliding boundaries (SL):

$$U = 0, \quad \left(\frac{\mathrm{i}\pi k}{2h}\right) U + W' = 0 \qquad \text{at } x = \pm h \tag{2.25}$$

Inextensional boundaries (IN):

$$W = 0, \quad aU' + \left(\frac{\mathrm{i}\pi k}{2h}\right) cW = 0 \qquad \text{at } x = \pm h \tag{2.26}$$

The prime ($'$) denote here differentiation with respect to the x coordinate.

Based on the symmetry of the problem it can be observed that the middle plane ($x = 0$) behaves as a sliding boundary (SL) for symmetric modes (2.14), and as an inextensional boundary (IN) for antisymmetric modes (2.15). Hence, with due account for the appropriate width ($h/2$) in each half field, we obtain also solutions for the mixed boundary conditions FR/SL, FR/IN, CL/SL, CL/IN, SL/IN.

The transverse velocity profiles (2.14)–(2.15) should comply with the boundary data (2.23)–(2.26), leading in each case to the vanishing of a 2×2 determinant at admissible solutions for k.

3. Compliance with boundary data and frequency maps

We now turn to a detailed investigation of the frequency spectra characterizing the prestrained plate, at various combinations of ideal boundary data over the long faces. The analysis concentrates on the full space of solutions for both propagating and evanescent waves, while axially growing modes are excluded from the discussion in view of Sommerfeld's radiation principle.

Three different compressible, hyperelastic, solids are addressed as a representative sample of material response. Their instantaneous moduli (2.3) are derived and discussed in Appendix A. We have chosen to present here numerical results for the standard Blatz–Ko model (BK) and for two vulcanized foam rubbers: A highly compressible natural rubber (S1) and a nearly incompressible synthetic rubber (S2).

Frequencies that admit the solution $k = 0$ are known as the cut-off frequencies, common to any boundary data, and have a special role in assessing the axial depth of penetration of evanescent waves. They are detailed in Appendix B for the hyperelastic materials considered here, with emphasis on the influence of prestrain on the two families of cut-off frequencies.

3.1. Free boundaries

Admissible wave numbers k at each given frequency Ω are determined from (2.23) by the transcendental equation

$$\tanh\left(\Gamma_1 \frac{\pi k}{2}\right) - \left(\frac{Q_1}{Q_2}\right)^{\pm 1} \tanh\left(\Gamma_2 \frac{\pi k}{2}\right) = 0 \tag{3.1}$$

where the (+) and (−) signs correspond to symmetric and antisymmetric modes, respectively, and

$$Q_p = \frac{a\Gamma_p + \mathrm{i}c\eta_p}{\eta_p \Gamma_p + i}, \quad p = 1, 2. \tag{3.2}$$

Eq. (3.1) is the quasi-linear analogue of the Rayleigh–Lamb equation derived under the assumptions of linear elasticity and solved completely by Mindlin (1960). An equivalent equation to (3.1) has been derived independently by Ogden and Roxburgh (1993) for incompressible materials and by Roxburgh and Ogden (1994) for compressible materials.

Eq. (3.1) has been solved numerically to trace permissible values of k for given frequency Ω, material moduli and initial stretch λ. The standard Muller method (e.g., Press et al., 2001) is employed to yield a finite set of smallest complex eigenvalues in the prestrain range of $1 < \lambda < 2.3$ and frequency range $0 < \Omega < 8$. Among the complex and the imaginary eigenvalues detected by the numerical routine, the only eigenvalues retained here are the first few in ascending order of the imaginary part.

Accuracy of the numerical scheme has been checked and confirmed by (a) recovering the quasistatic results of Karp and Durban (2002) obtained with $\Omega = 0$ at different levels of prestretch, (b) recalculating the real and the complex wave numbers k at the stress free state ($\lambda = 1$) with $v = 0.31$ and 0.25 and comparing that data with the original results of Mindlin (1960) and Achenbach (1973), (c) checking the cut-off frequencies (B.3) at the limit $k = 0$, and (d) verifying the agreement with the asymptotic expansions obtained at the long wavelength limit.

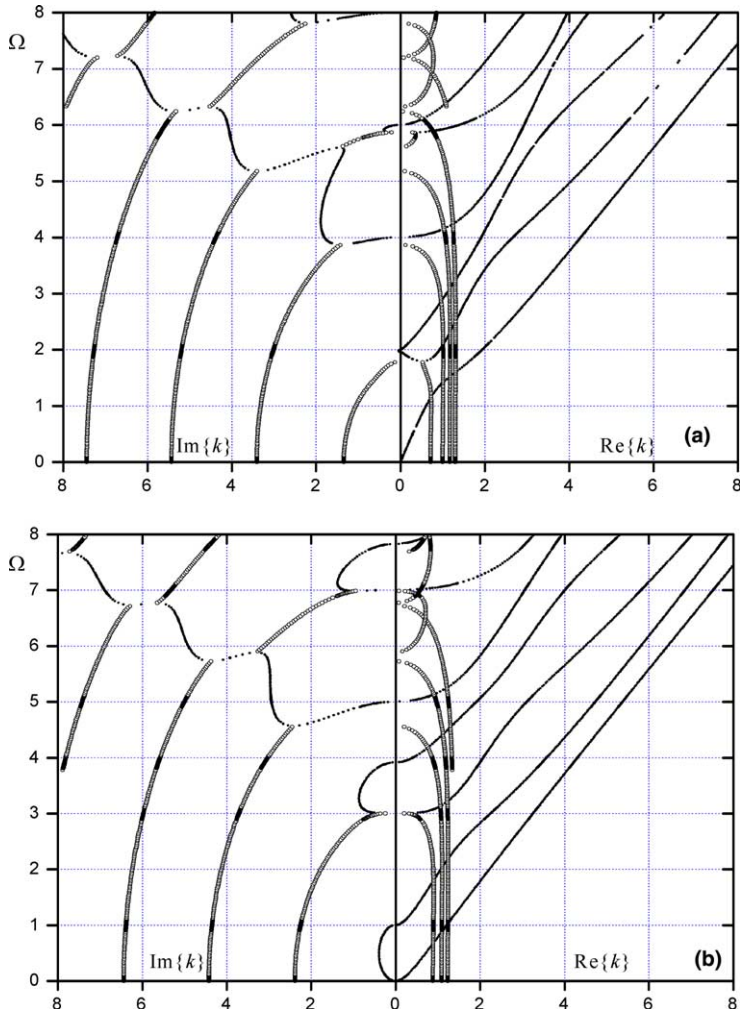

Fig. 2. Frequency maps for the highly compressible rubber S1 at the stress free configuration ($\lambda = 1$) with free boundaries. Thin lines (composed of black dots) indicate real and purely imaginary branches. Thick lines (composed of hollow circles) indicate complex branches (two curves for each eigenvalue). (a) Symmetric modes, (b) antisymmetric modes.

Figs. 2 and 3 display the frequency spectrum for the highly compressible rubber (S1) given in (A.6), at the stress free state ($\lambda = 1$) and with initial stretch of $\lambda = 1.4$, respectively. The equivalent results for the nearly incompressible rubber (S2) defined by (A.7) are shown in Figs. 4 and 5. Typical frequency maps for the BK material (A.5) are displayed in Fig. 6 and can be compared with Figs. 3 and 5, and with the linear elastic results for $\nu = 0.25$ given by Achenbach (1973). The stretch $\lambda = 1.4$ has been chosen here as representative to illustrate the effect of prestress on the frequency maps. Due to the complex-value nature of the eigenvalues, each branch on the figures is actually composed of dots with intervals dictated by the increments of Ω in the numerical routine.

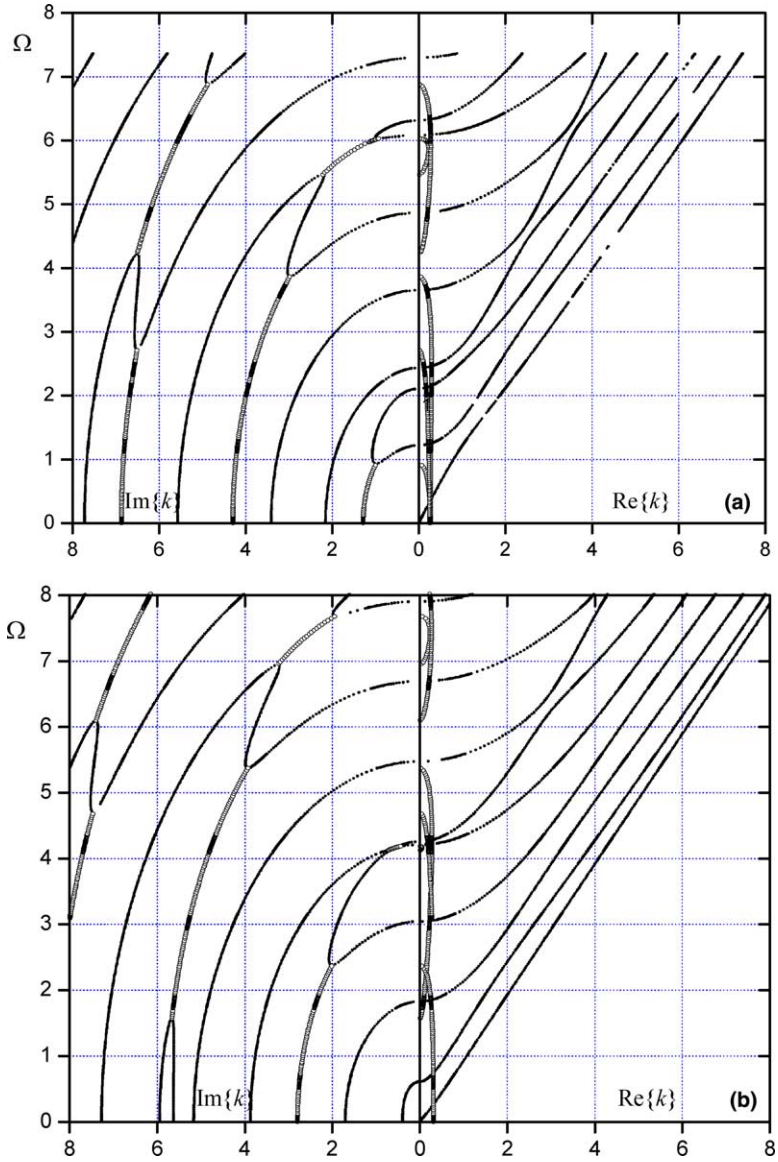

Fig. 3. Frequency maps for the S1 solid at initial stretch of $\lambda = 1.4$ with free boundaries. Nomenclature as in Fig. 2. (a) Symmetric modes, (b) antisymmetric modes.

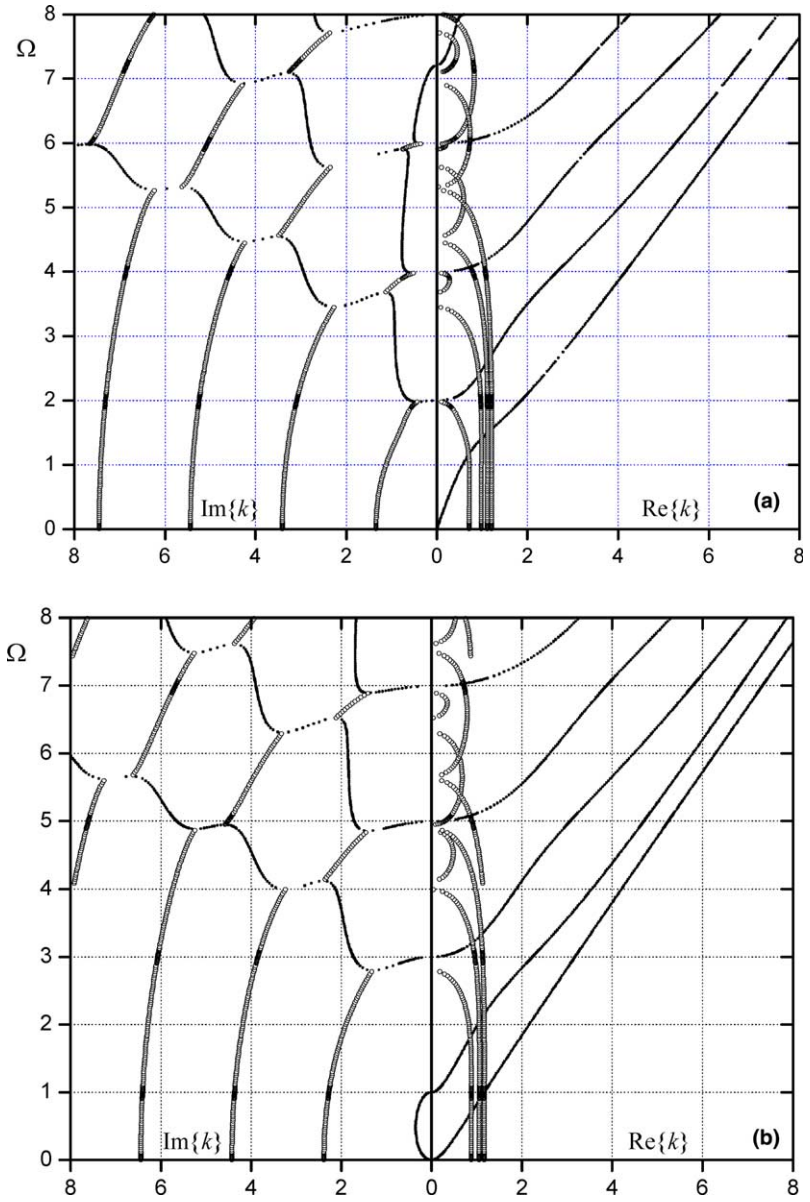

Fig. 4. Frequency maps for the nearly incompressible rubber S2 at the stress free configuration ($\lambda = 1.0$), with free boundaries. Nomenclature as in Fig. 2. (a) Symmetric modes, (b) antisymmetric modes.

The general pattern of frequency spectrum obtained previously in linear elasticity (Mindlin, 1960), consisting of propagating (real k) and evanescent (complex or purely imaginary k) waves, is preserved here regardless of prestrain level. Namely, only one propagating mode is possible at low frequencies for each symmetric and antisymmetric field, accompanied by an infinite number of possible evanescent waves. These propagating modes are the fundamental modes, which at low frequency correspond to solutions obtained under the assumptions of beam theory. As the frequency increases, one propagating mode is added at each surpass of a cut-off frequency. Other common features observed in a linear elastic analysis, such as existence

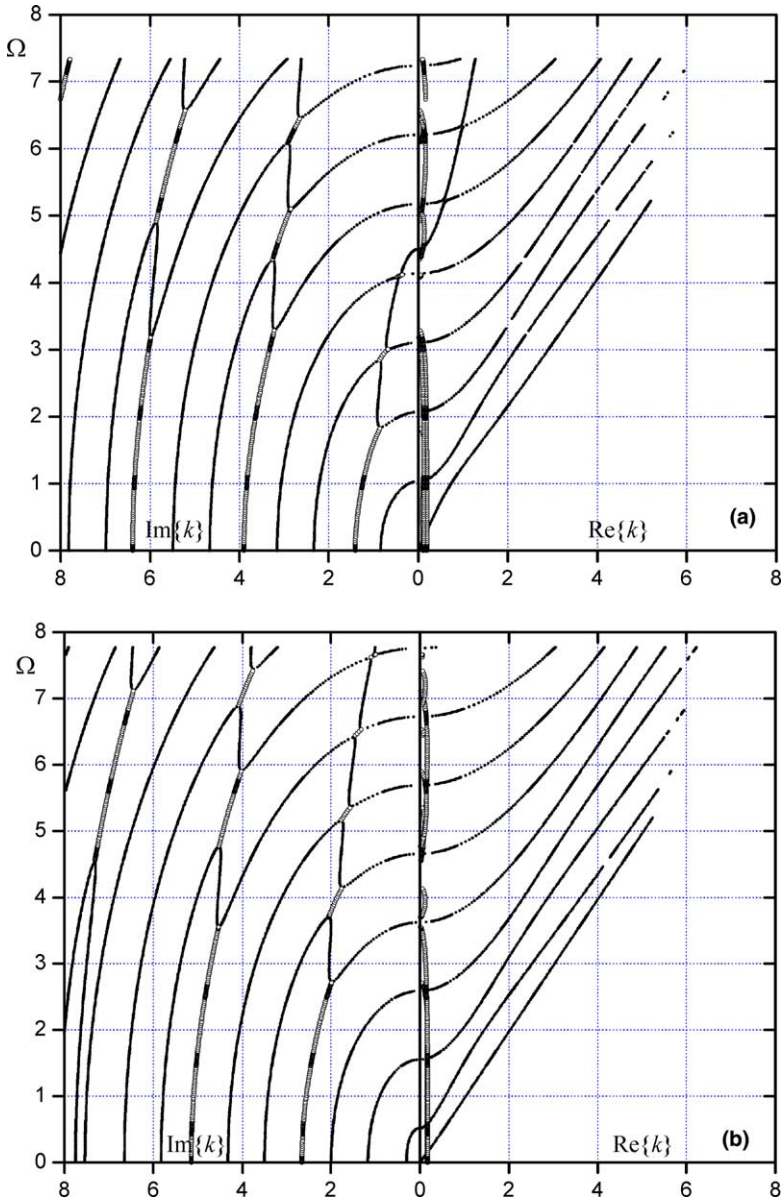

Fig. 5. Frequency maps for the nearly incompressible rubber S2 at initial stretch of $\lambda = 1.4$, with free boundaries. Nomenclature as in Fig. 2. (a) Symmetric modes, (b) antisymmetric modes.

of negative group velocity, merging of the complex branches with either purely real or purely imaginary branches at their minima or maxima points, can be observed in the figures given here, and will not be discussed in the present communication.

At sufficiently low values of Ω the wave numbers approach the quasistatic eigenvalues $k_s \equiv k(\Omega = 0)$ discussed by Karp and Durban (2002). It can be verified from 3.1 that when $\Omega^2 \ll 1$ the roots admit the expansion (except near the origin $\Omega = 0$, $k = 0$)

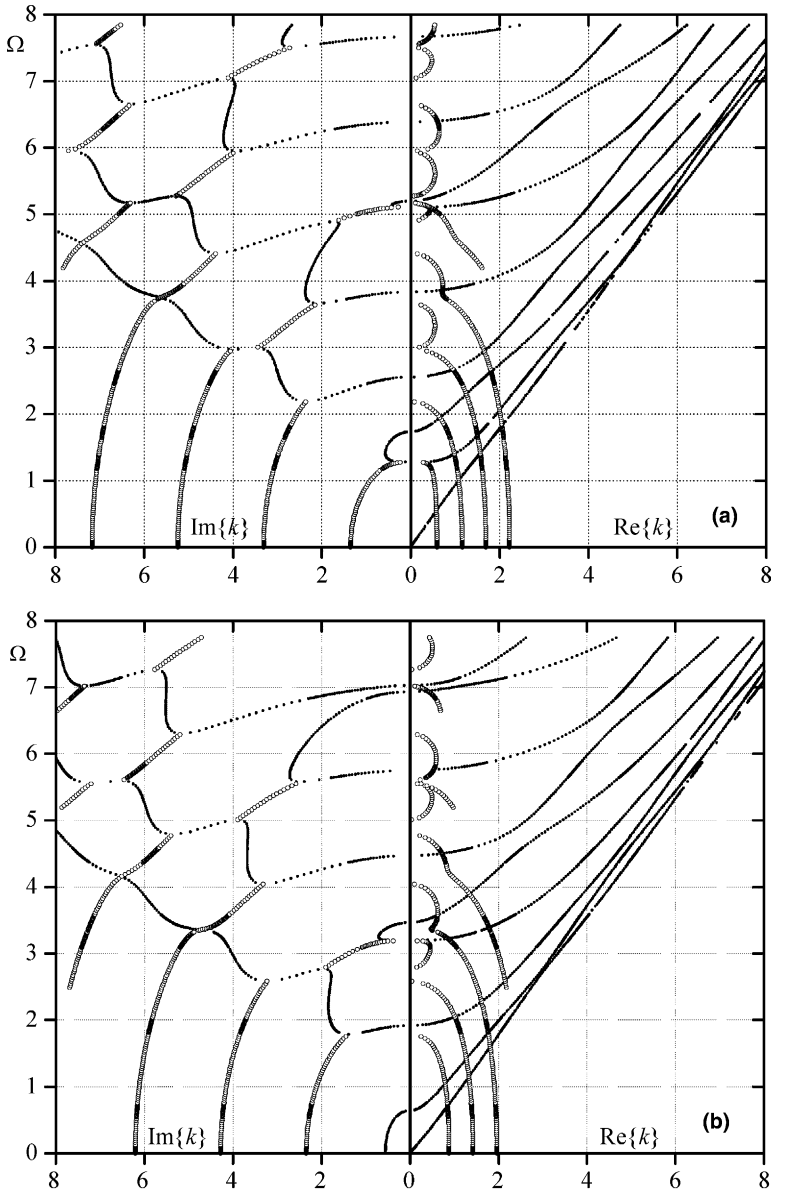

Fig. 6. Frequency maps for the foam rubber BK at initial stretch of $\lambda = 1.4$, with free boundaries. Nomenclature as in Fig. 2. (a) Symmetric modes, (b) antisymmetric modes.

$$k \approx k_s + k_1 \Omega^2 \tag{3.3}$$

implying that $\partial k/\partial \Omega$ vanishes at $\Omega = 0$ as in the case of linear elasticity (Achenbach, 1973). Both k_s and the coefficient k_1 in (3.3) depend of course on initial stretch and material moduli.

Similarly, near the cut-off frequencies (B.3), where $|k^2| \ll 1$, the roots of (3.1) behave essentially like

$$\Omega_1 k^2 \approx \Omega - \Omega_c \tag{3.4}$$

where Ω_c denotes any of the cut-off frequencies (B.3) and coefficient Ω_1 depends on initial stretch and material moduli. Notice that while both Ω_c and Ω_1 in (3.4) are real and positive, k can become purely imaginary. That implies that for $\Omega > \Omega_c$ the wave number is real and associated with a propagating wave, while for $\Omega < \Omega_c$ the wave number is purely imaginary representing an evanescent wave as can be observed in Figs. 2–6 (and in subsequent figures as well).

It is instructive to recall at this point the general nature of propagating modes emerging at the cut-off frequency. The non-dimensional phase velocity of the wave is defined as $C = \Omega/k$. From (3.4), which is valid for small k, we find that the phase velocity tends to infinity at a frequency infinitesimally above the cut-off frequency. The same result for incompressible materials is reported by Rogerson (1997). The non-dimensional group velocity, on the other hand, defined by $V_g = \partial\Omega/\partial k$, vanishes at the same cut-off frequency in agreement with the observation made by Pichugin and Rogerson (2001) for incompressible materials. That property has been explained by Achenbach (1973) as a feature reflecting the mathematical structure of (3.1) and providing a defining relation between Ω^2 and k^2.

For the fundamental modes, when $\Omega^2 \ll 1$ and $|k^2| \ll 1$, we can use the standard expansion of $\tanh\gamma \approx \gamma - 1/3\gamma^3$ (for $\gamma^2 \ll 1$) and replace the transcendental equations (3.1) by much simpler versions valid near the origin. Thus, for symmetric mode we have the elegant expression

$$k \approx \sqrt{\frac{a\beta}{ab - c^2}}\Omega \tag{3.5}$$

predicting the linear non-dispersive ($C = V_g$) relation observed in Figs. 2a, 3a, 4a, 5a and 6a. That result degenerates to the linear elastic case upon substitution of the stress free state relations (A.8), resulting in (Achenbach, 1973)

$$k \approx \sqrt{\frac{1 - \nu_0}{2}}\Omega \tag{3.6}$$

Of particular interest is the specification of relation (3.5) for prestrain near necking instability, where $ab - c^2 = 0$ as discussed in Durban and Karp (1992) in the context of quasi-static response. For example, with the BK material (A.9) relation (3.5) takes the form

$$k \approx \sqrt{\frac{3}{9R - 1}}\Omega \quad \text{with } R \equiv \lambda^{-8/3} \tag{3.7}$$

Now, the ultimate tensile load is obtained when $R = 1/9$ which corresponds to the ultimate stretch $\lambda_u \approx 2.28$ (notice maximum in load curve at that stretch in Fig. 1). It follows that for stretch λ slightly below λ_u the wave constant (3.7) is, at low frequencies,

$$k \approx \sqrt{\frac{9\lambda_u}{8(\lambda_u - \lambda)}}\Omega \tag{3.8}$$

indicating that both phase and group velocities of that propagating fundamental mode are approaching zero near necking.

Applying a similar expansion for the antisymmetric fundamental mode near the origin where $\Omega^2 \ll 1$ and $|k^2| \ll 1$, we find from (3.1) that at any finite prestretch λ

$$k \approx \sqrt{\frac{\beta}{\beta - \alpha}}\Omega = \sqrt{\frac{\mu}{\sigma} + \frac{1}{2}}\Omega, \quad \lambda > 1 \tag{3.9}$$

while at the stress free configuration the leading term is given by

$$k^2 \approx \pm\frac{\sqrt{6}}{\pi}\sqrt{1 - \nu_0}\Omega, \quad \lambda = 1 \tag{3.10}$$

in complete agreement with Achenbach (1973). A relation, equivalent to (3.9) for an incompressible material, is deduced by Rogerson (1997).

Comparison of relations (3.9) and (3.10) suggest an interesting influence of prestretch on the nature of the fundamental flexural mode. While in the absence of prestretch relation (3.10) indicates dispersive behaviour of that mode, relation (3.9) points to the absence of dispersion upon application of prestress of any magnitude. A similar observation has been made by Johnson and Chen (1989) for an aluminum plate, though no explicit relation is given and by Kaplunov et al. (2000) for an incompressible rubber-like solid. The dispersive relation (3.10) can be observed in Figs. 2b and 4b upon noting the parabolic shape of the fundamental mode near the origin. In Figs. 3b, 5b and 6b the same mode shows linear dependence of Ω on k, in agreement with relation (3.9).

With the BK definitions (A.9) relation (3.9) takes a the simple form

$$k \approx \sqrt{\frac{1}{1-R}}\Omega \quad \text{with } R \equiv \lambda^{-8/3} \tag{3.11}$$

implying a highly oscillatory behaviour near the stress free state. In fact, the first order expansion of (3.9) in powers of $(\lambda - 1)$ gives, for the entire family (A.2),

$$k \approx \sqrt{\frac{1-\nu_0}{2(\lambda-1)}}\Omega, \quad \lambda > 1 \tag{3.12}$$

Expressions (3.5) and (3.12) reflect the sensitivity of dynamic response near points of instability: necking in tension and buckling of a semi-infinite plate in compression.

The asymptotic derivations detailed here are limited to the long wave length region and brought here in support and generalization of the numerical results. Further asymptotic results for the propagating modes in the short wave length limit have been given by Rogerson (1997), Kaplunov et al. (2002) and in other works related to surface waves (e.g., Chadwick and Jarvis, 1979).

3.2. Clamped boundaries

The case where no velocity component is allowed to develop along the boundaries (2.24) represents the stiffest possible constraint. The equations for wave numbers k are here obtained in the form

$$\tanh\left(\Gamma_1 \frac{\pi k}{2}\right) - \left(\frac{\eta_1}{\eta_2}\right)^{\pm 1} \tanh\left(\Gamma_2 \frac{\pi k}{2}\right) = 0 \tag{3.13}$$

where the $(+)$ and $(-)$ signs correspond to symmetric and antisymmetric modes, respectively, and (η_1, η_2) are given in (2.16).

Numerical solutions of (3.13) have been checked against the quasistatic results in (Karp and Durban, 2002). Sample frequency maps are displayed in Figs. 7 and 8 for the BK material, Figs. 9 and 10 for the S1 material, and Figs. 11 and 12 for the S2 material, respectively. Unlike the case of free boundaries, in the range of low frequencies no propagating mode can develop (see Kaplunov, 1995, for same condition in the linear elastic case). The two fundamental modes are eliminated here by the constraint imposed by the clamped boundaries.

It is clearly seen that the pattern of frequency maps for the symmetric modes of a clamped plate (Figs. 8a, 9a and 10a) resembles that of antisymmetric modes for a plate with free boundaries (Figs. 6b, 2b and 3b) for the highly compressible solids BK and S1. The same similarity of patterns exists between Figs. 8b, 9b, 10b and 6a, 2a, 3a (except for the fundamental modes in both cases). For the nearly incompressible solid, S2, the similarity is less pronounced due to material resistance to develop dilatational waves. Comparison of Figs. 11b and 12b for a plate with fixed faces and with Figs. 4a and 5a for a plate with free faces,

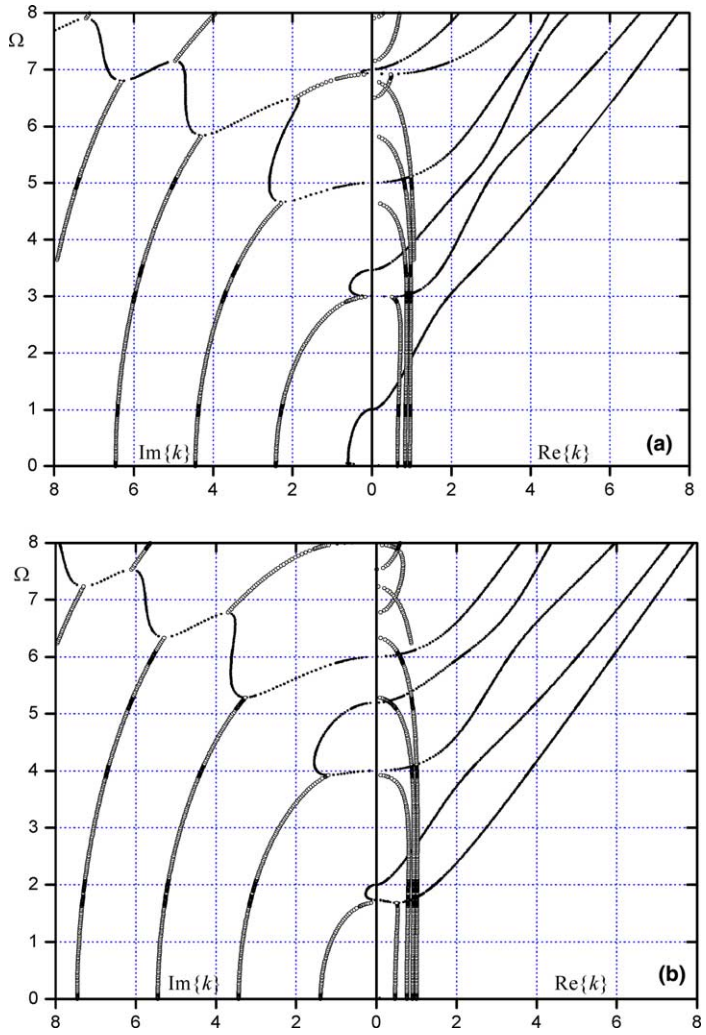

Fig. 7. Frequency maps for the BK solid at the stress free configuration $\lambda = 1.0$, with clamped boundaries. Nomenclature as in Fig. 2. (a) Symmetric modes, (b) antisymmetric modes.

reveals that the evanescent waves are almost identical for the S2 solid, while the propagating modes have an asymptotic limit in the long wave region (small k). The asymptote here is the longitudinal wave in an infinite medium (3.22), shown as a straight line in Fig. 15b, and can be related to the "unexpected" pattern noted by Kaplunov and Nolde (2002).

Due to the aforementioned similarity, we do not explore further the case of clamped boundaries in detail. It is worth noting, however, that expressions similar to (3.3) and (3.4) hold here as well, and that at any given frequency there is only a limited number of propagating waves with an infinite number of evanescent waves. Asymptotic derivations for propagating modes in an incompressible material can be found in Nolde and Rogerson (2002), and in Kaplunov and Nolde (2002) for a nearly incompressible plate.

One interesting aspect of frequency maps exclusively characteristic of plates with clamped faces is worth to mention. A careful observation of the symmetric frequency maps for the nearly incompressible rubber S2

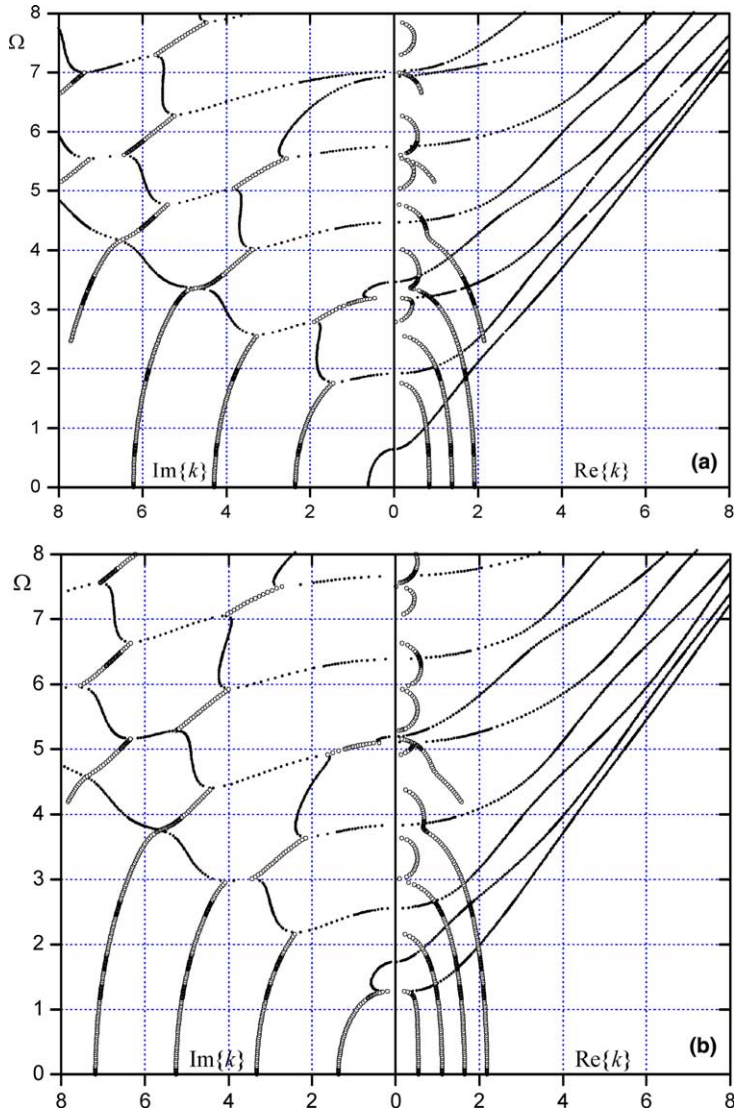

Fig. 8. Frequency maps for the BK solid at initial stretch of $\lambda = 1.4$, with clamped boundaries. Nomenclature as in Fig. 2. (a) Symmetric modes, (b) antisymmetric modes.

(Figs. 11a and 12a) reveal that the real branches originate at cut-off frequencies with an "S" shape. It can be shown that the middle part of the "S" shape of all branches lays on a line defined by (3.22) shown in Figs. 13b and 15b for the S2 material. The upper bend-down of the "S" shape admits an asymptotic expansion at the limit of nearly incompressible materials along the lines given by Kaplunov and Nolde (2002) for a linearly elastic material.

Observing the volume ratio (A.13) we may argue that for nearly incompressible solids $n \to \infty$. Now, for large values of n we have from Eqs. (A.3) that the moduli a, b, c, approach the same asymptotic limit of $n\sum_j c_j m_j \lambda^{-m_j}$ which is much larger than α and β of (2.6). Searching now for asymptotes where $\Omega^2 \gg k^2$ we approximate (2.20) by the leading terms

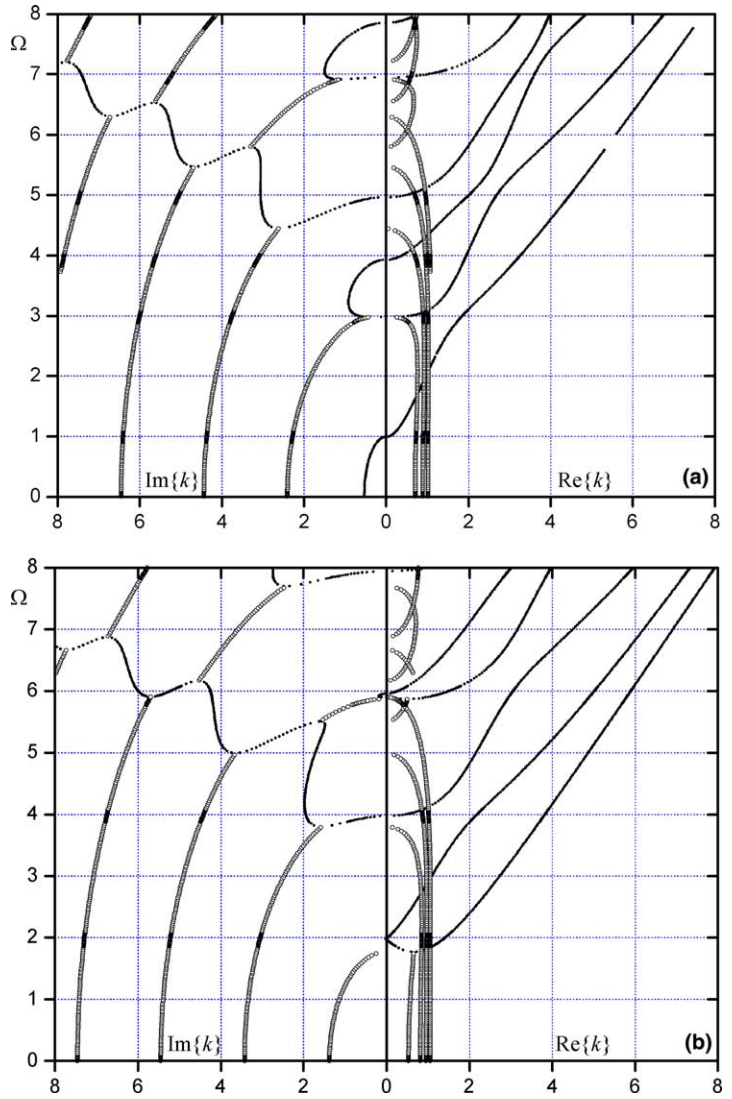

Fig. 9. Frequency maps for the S1 solid at the stress free configuration $\lambda = 1.0$, with clamped boundaries. Nomenclature as in Fig. 2. (a) Symmetric modes, (b) antisymmetric modes.

$$\Gamma_1^2 \approx -\frac{\beta}{\alpha}\left(\frac{\Omega}{k}\right)^2 + \frac{\beta(a-\alpha)+(c+\alpha)^2}{\alpha(a-\alpha)}, \quad \Gamma_2^2 \approx -\frac{\beta}{a}\left(\frac{\Omega}{k}\right)^2 + \frac{\beta(a-\alpha)+(c+\alpha)^2}{a(a-\alpha)} \tag{3.14}$$

A further substitution of these expressions in the symmetric eigenvalues equation (3.13) gives the leading order terms

$$\frac{\beta(a-\alpha)+(c+\alpha)^2}{a(a-\alpha)}\left(\sqrt{\frac{\beta}{\alpha}}\frac{\pi}{2}\Omega\right) - \frac{(c+\alpha)^2}{(c-\alpha)^2}\tan\left(\sqrt{\frac{\beta}{\alpha}}\frac{\pi}{2}\Omega\right) = \sqrt{\frac{\beta}{\alpha}}\left(\frac{\beta}{a}\right)\frac{\pi}{2}\left(\frac{\Omega}{k}\right)^3 \tag{3.15}$$

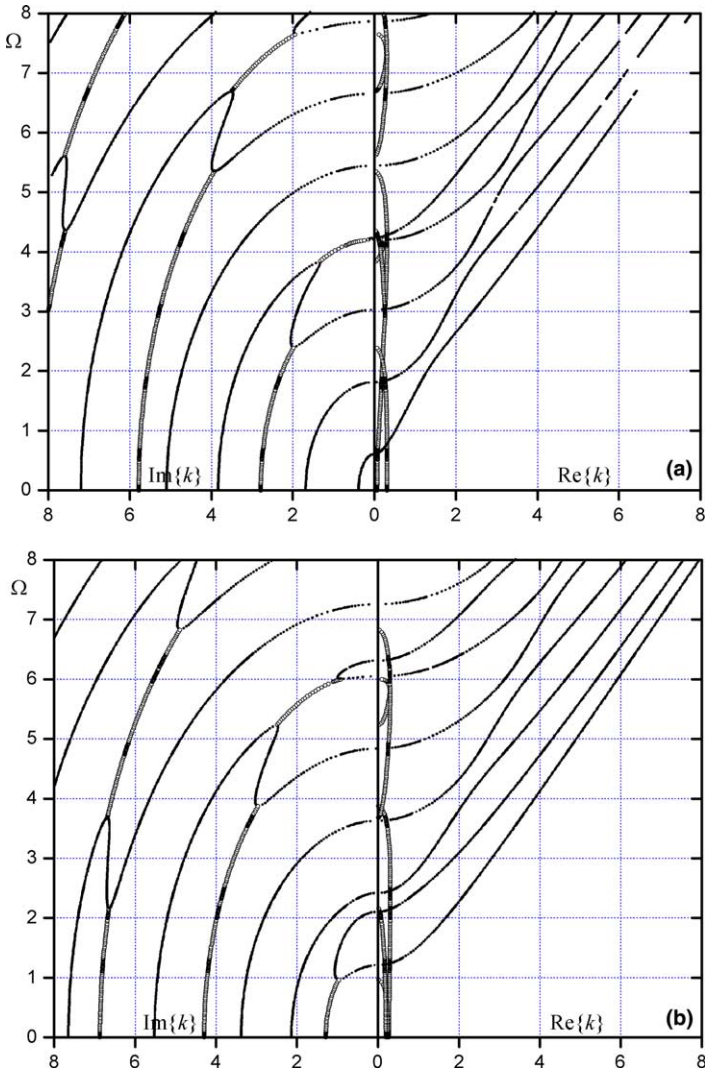

Fig. 10. Frequency maps for the S1 solid at initial stretch of $\lambda = 1.4$, with clamped boundaries. Nomenclature as in Fig. 2. (a) Symmetric modes, (b) antisymmetric modes.

At the stress free configuration we recover the equation (Kaplunov and Nolde, 2002)

$$\frac{\pi}{2}\Omega - \tan\left(\frac{\pi}{2}\Omega\right) = \frac{1}{2(n+1)}\frac{\pi}{2}\frac{\Omega^3}{k^3} \quad \text{with } n = \frac{v_0}{1-2v_0} \tag{3.16}$$

Thus, as $n \to \infty$ the asymptotical values of Ω are determined by $\frac{\pi}{2}\Omega - \tan(\frac{\pi}{2}\Omega) = 0$.

For finite strains, with $n \to \infty$ we find the limiting frequencies from the equation (since $\beta/\alpha \to \lambda^4$)

$$\frac{\pi}{2}\lambda^4\Omega = \tan\left(\frac{\pi}{2}\lambda^4\Omega\right) \tag{3.17}$$

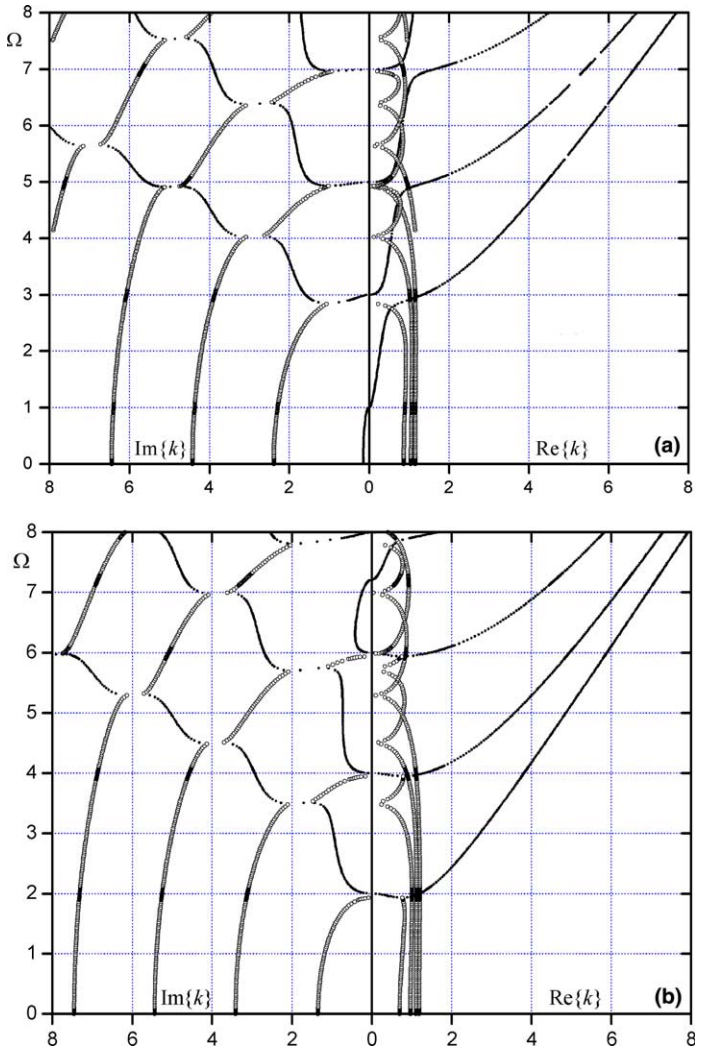

Fig. 11. Frequency maps for the S2 solid at the stress free configuration $\lambda = 1.0$, with clamped boundaries. Nomenclature as in Fig. 2. (a) Symmetric modes, (b) antisymmetric modes.

Numerical solution of (3.17) and its linear counterpart is straightforward and agrees with the numerical results obtained here. Solution of (3.17) for high frequencies Ω, a region where the initial assumption of $\Omega^2 \gg k^2$ is more valid, gives limiting frequencies that approach the cut-off frequency values. The effect of compressibility on the "S" shape obtained by Kaplunov and Nolde (2002), can be observed in Figs. 7 and 9 representing the linear elastic limit of the highly compressible materials considered here.

3.3. Sliding boundaries

The boundary conditions (2.25) generate here the transcendental equations

$$\sinh\left(\Gamma_1 \frac{\pi k}{2}\right) = 0 \quad \text{and} \quad \sinh\left(\Gamma_2 \frac{\pi k}{2}\right) = 0 \tag{3.18}$$

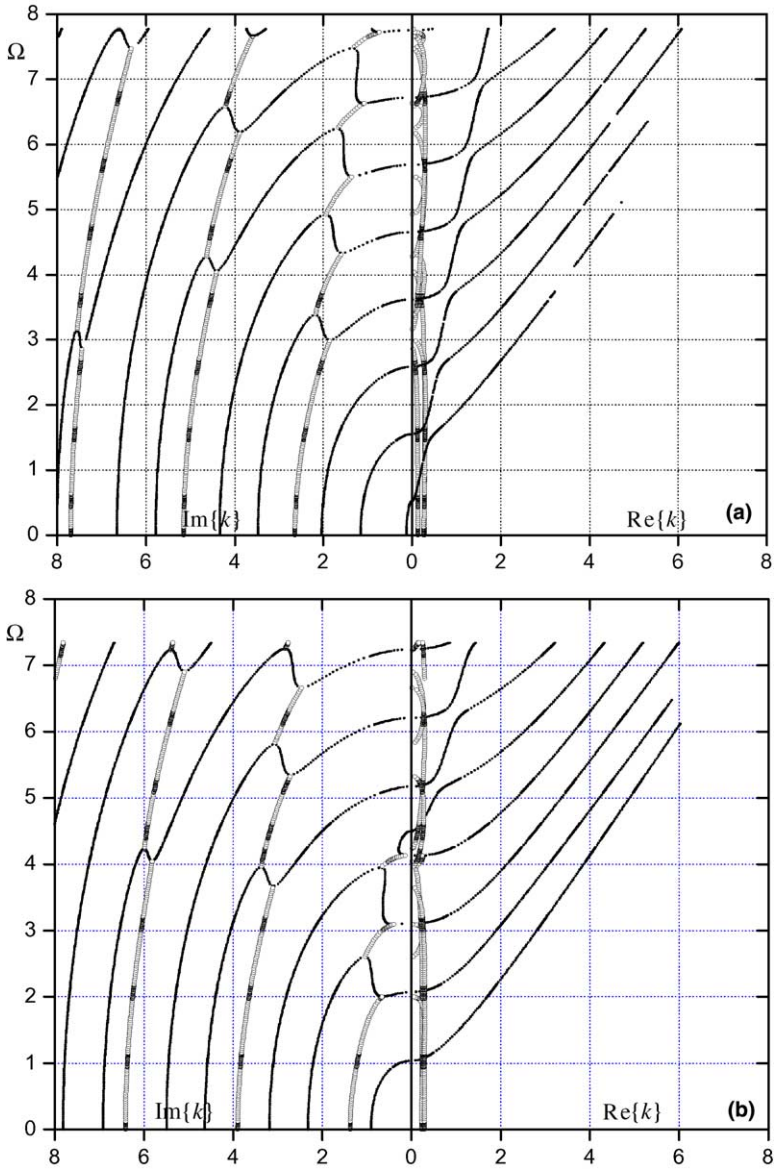

Fig. 12. Frequency maps for the S2 solid at initial stretch of $\lambda = 1.4$, with clamped boundaries. Nomenclature as in Fig. 2. (a) Symmetric modes, (b) antisymmetric modes.

for symmetric modes, and

$$\cosh\left(\Gamma_1 \frac{\pi k}{2}\right) = 0 \quad \text{and} \quad \cosh\left(\Gamma_2 \frac{\pi k}{2}\right) = 0 \tag{3.19}$$

for antisymmetric modes. Eqs. (3.18) and (3.19) admit the solutions $\Gamma_j k = \mathrm{i}N$ $(j = 1, 2)$, where $N = 0, 2, 4, \ldots$ for symmetric modes (3.18) and $N = 1, 3, 5, \ldots$ for antisymmetric modes (3.19). A further use of relations

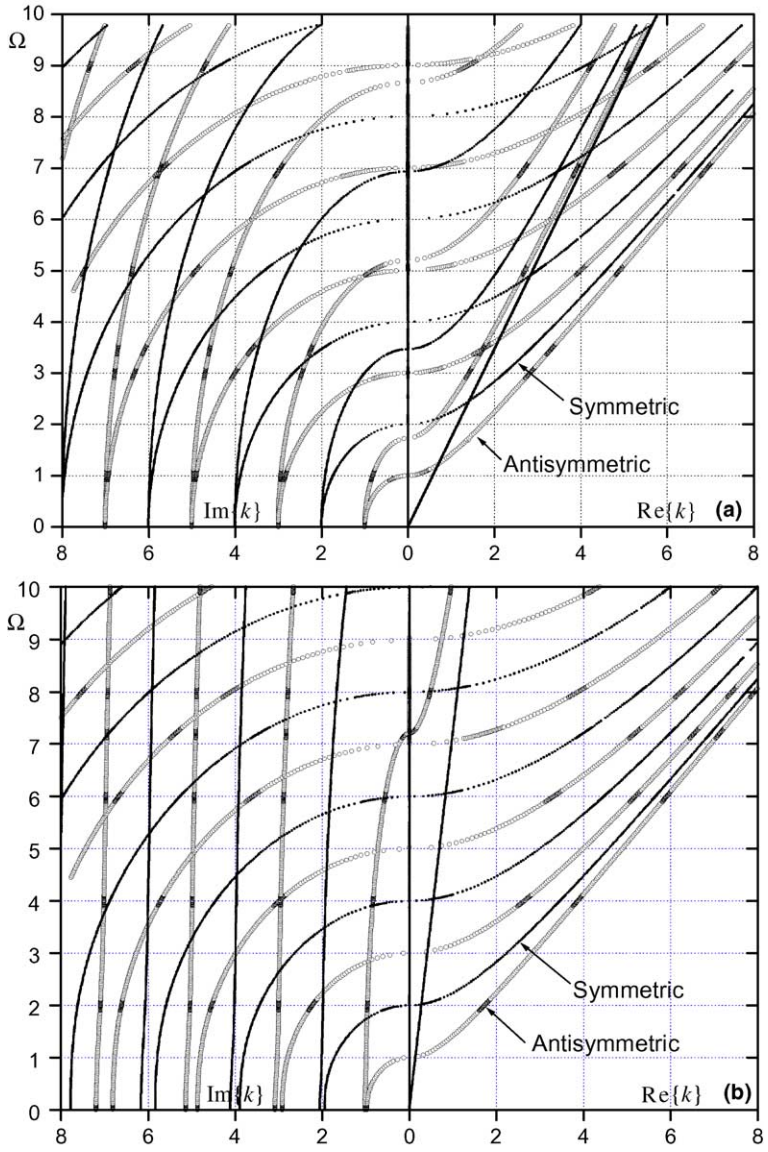

Fig. 13. Frequency maps at the stress free configuration $\lambda = 1.0$, with sliding boundaries. Thin lines indicate symmetric modes and thick lines indicate antisymmetric modes. (a) BK material. (b) S2 material.

(2.20) shows that the solutions of all four equations (3.18) and (3.19) follow from the common algebraic equation:

$$(b\beta)k^4 + [dN^2 - \beta(b+\beta)\Omega^2]k^2 + [a\alpha N^4 - \beta(a+\alpha)N^2\Omega^2 + \beta^2\Omega^4] = 0 \tag{3.20}$$

where even integers $N = 0, 2, 4, \ldots$ correspond to symmetric fields and odd integers $N = 1, 3, 5, \ldots$ correspond to antisymmetric fields. The solution of (3.20) is immediate and fairly simple. In the absence of prestretch we recover the known linear elastic results (Achenbach, 1973)

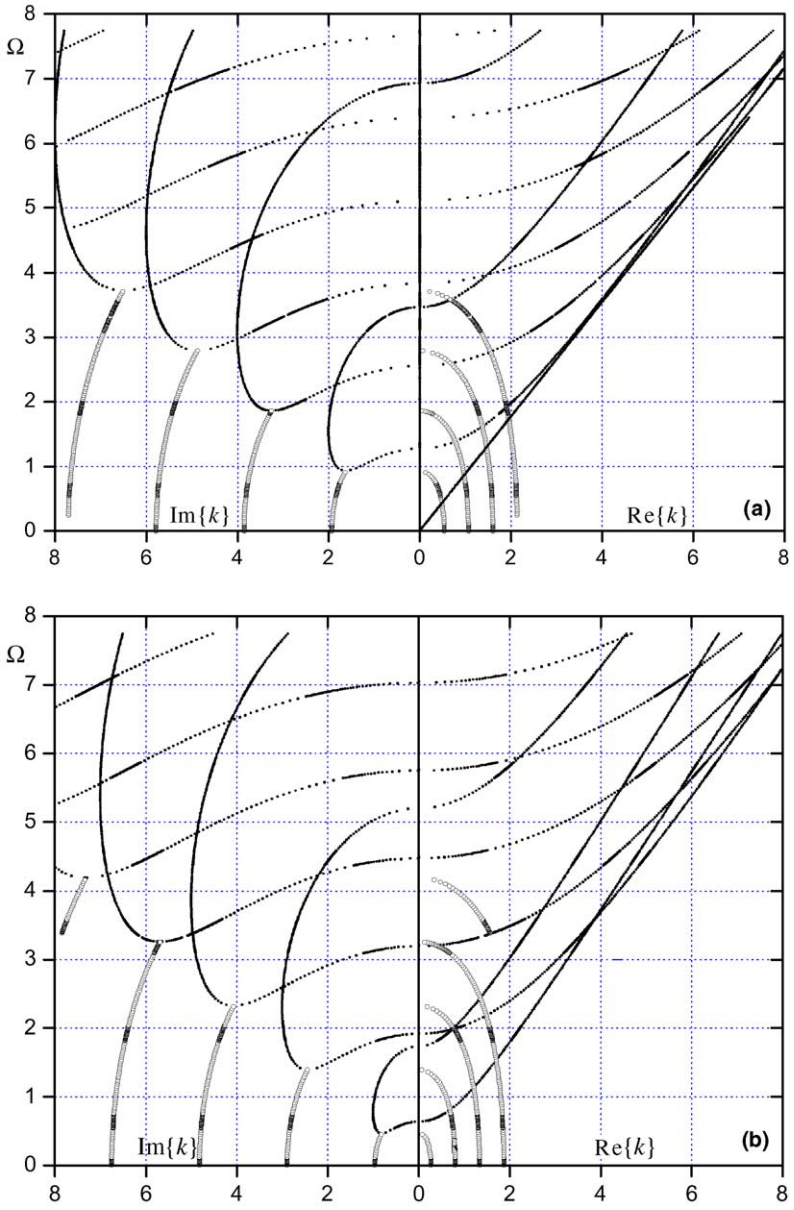

Fig. 14. Frequency maps for the BK solid at initial stretch of $\lambda = 1.4$ with sliding boundaries. Nomenclature as in Fig. 2. (a) Symmetric modes, (b) antisymmetric modes.

$$k^2 = \frac{1-2\nu_0}{2(1-\nu_0)}\Omega^2 - N^2, \quad N = 0, 1, 2, 3, 4, \ldots \tag{3.21a}$$

$$k^2 = \Omega^2 - N^2, \quad N = 1, 2, 3, 4, \ldots \tag{3.21b}$$

All roots are here either purely imaginary or purely real, as illustrated in Fig. 13 for the BK and S2 materials in the stress free state. Complex roots appear with finite stretch for the BK material (Fig. 14), but not for the S1 and S2 materials (Fig. 15).

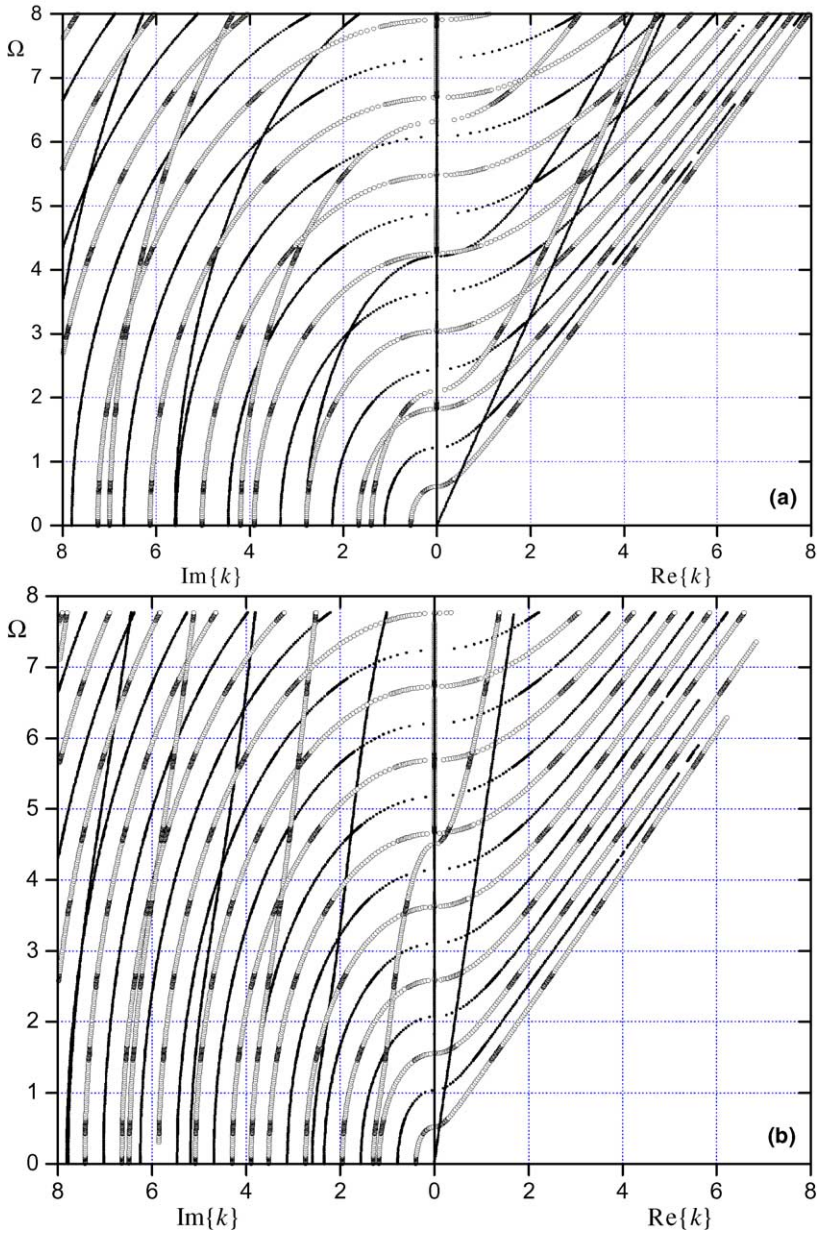

Fig. 15. Frequency maps at initial stretch of $\lambda = 1.4$ with sliding boundaries. Nomenclature as in Fig. 13. (a) S1 material. (b) S2 material.

For symmetric modes there is just one propagating wave below the first cut-off frequency (Figs. 13, 14a and 15), given by the solution of (3.20) for $N = 0$,

$$k = \sqrt{\frac{\beta}{b}}\Omega \tag{3.22}$$

That solution corresponds to non-dispersive dilatational waves for an infinite medium (not possible in incompressible solids) and is shown in Figs. 13, 14b and 15 as a straight line. The other solution ($k = \Omega$) of (3.20) for $N = 0$ is not physically admissible for the boundary data under consideration. For the BK material relation (3.22) reads $k = (\lambda^{4/3}/\sqrt{3})\Omega$.

For antisymmetric modes (Figs. 13, 14b and 15) only evanescent waves are possible if Ω is below the first cut-off frequency. However, as Ω increases the number of propagating modes increases as well (for both symmetric and antisymmetric modes), in common with previous observations for free and clamped boundaries.

The simple algebraic structure of Eqs. (3.20) permits the derivation of elegant relations for key points in the frequency map. Just to give an example, coefficient Ω_1, in the near cut-off frequency expansion (3.4), takes here the form

$$\Omega_1 = -\frac{(a-\alpha)\beta + (c+\alpha)^2}{2(a-\alpha)\sqrt{a\beta}}\left(\frac{1}{N}\right) \quad \text{near } \Omega = \Omega_{CL} \tag{3.23a}$$

$$\Omega_1 = -\frac{(\alpha-a)b + (c+\alpha)^2}{2(\alpha-a)\sqrt{a\beta}}\left(\frac{1}{N}\right) \quad \text{near } \Omega = \Omega_{CT} \tag{3.23b}$$

where the cut-off frequencies are given in (B.3) with $m, n = N$. Relations (3.23) imply that Ω_1 decreases with N as can indeed be verified from Figs. 13–15 (Ω_1 is correlative to the group velocity, $V_g = 2\Omega_1 k$ from (3.4)). For real values of k we find from (3.20) the two asymptotes are

$$k = \Omega\left[1 - \frac{a(b-\beta) - (c+\alpha)^2}{2(b-\beta)\beta}\left(\frac{N}{\Omega}\right)^2\right] \tag{3.24a}$$

$$k = \sqrt{\frac{\beta}{b}}\Omega\left[1 - \frac{a(b-\beta) - (c+\alpha)^2}{2(b-\beta)\beta}\left(\frac{N}{\Omega}\right)^2\right] \tag{3.24b}$$

both valid for $\Omega^2 \gg k^2$.

3.4. Inextensional boundaries

The eigenvalue equations obtained from the boundary data (2.26) are identical with those of sliding boundaries (3.18) and (3.19), apart from the exchange of symmetric modes with antisymmetric modes. Thus, eigenvalues k are obtained from (3.20) with even values of N describing antisymmetric modes and odd values of N describing symmetric modes. The analogue of (3.22) is here obtained for the antisymmetric mode ($N = 0$) and is given by

$$k = \Omega \tag{3.25}$$

with the other solution for $N = 0$ being physically inadmissible. The non-dispersive wave described by (3.25) corresponds to a shear wave in an infinite medium.

3.5. Non-symmetric boundary conditions

Due to the symmetry of boundary conditions (2.9)–(2.12) we find that at the middle surface of the plate ($x = 0$) the symmetric fields (2.14) comply with the sliding condition (2.11) identically. Similarly, the antisymmetric fields (2.15) comply with the inextensional condition (2.12) at the mid-plane $x = 0$. Therefore, redefining the width of a free-inextensional plate as h, the frequency maps in Figs. 2a–6a can be considered as

a solution for the FR/SL plate where x in the solution (2.13) varies in the range $0 < x < h$. Although the wave number is the same as for the FR/FR plate, the depth of penetration is now related to a smaller plate width h (rather than $2h$). Consequently, the effective depth of penetration is twice as large as in the case of the FR/FR plate.

Similarly, the wave numbers in Figs. 2b–6b can be taken as a solution for the FR/IN plate, those in Figs. 7a–12a for the CL/SL plate, and those of Figs. 7b–12b for the CL/IN plate, where the effective depth of penetration is twice as large for the mixed boundary conditions.

4. Discussion

The frequency maps presented in the previous section reveal a considerable sensitivity of both propagating and evanescent waves to the frequency of the end disturbance and to the prestretch of the plate. However, the non-dimensionalized frequency Ω, defined in (2.19), is stretch dependent and it is therefore instructive to examine the influence of prestretch separately by considering the direct term of physical frequency. That separation is of importance for estimation of the proximity of any given frequency to cut-off frequencies (e.g. Pichugin and Rogerson, 2001), especially due to the fact that in many cases waves are induced by external generators having a fixed frequency spectrum.

To this end, we define the reference frequency (having dimensions of $\sqrt{N}/\mathrm{mm}$)

$$\omega^* \equiv \frac{2}{\pi}\sqrt{\rho_0}h_0\omega \tag{4.1}$$

where h_0—the initial undeformed thickness—is related to the deformed thickness by

$$\frac{h}{h_0} = \lambda^{-\frac{n}{n+1}} \tag{4.2}$$

for the entire hyperelastic family (A.2). It follows that ω^* is related to Ω by

$$\omega^* = \sqrt{\beta}\lambda^{\frac{2n+1}{2(n+1)}}\Omega \tag{4.3}$$

Thus, the reference cut-off frequencies (B.3) are given by

$$\omega^*_{\mathrm{cL}} = m\sqrt{a}\lambda^{\frac{2n+1}{2(n+1)}}, \quad \omega^*_{\mathrm{cT}} = n\sqrt{\alpha}\lambda^{\frac{2n+1}{2(n+1)}}, \qquad m,n = 1,2,3,\ldots \tag{4.4}$$

Fig. 16 shows the first cut-off reference frequencies ($m,n = 1$) at different levels of stretch λ, for the three materials. With the BK moduli (A.9) they take the simple form

$$\omega^*_{\mathrm{cL},1} = \sqrt{3\mu_0}\lambda^{-2/3}, \quad \omega^*_{\mathrm{cT},1} = \sqrt{\mu_0}\lambda^{-2/3} \tag{4.5}$$

By comparison with Fig. B.1, the physical cut-off frequencies display quite different dependence on the initial stretch. Moreover, the constitutive properties can reverse the effect of prestretch from monotonously decreasing (BK material in Fig. 16b) to increasing (S2 material) the frequency, or even make it non-monotonous (S1 material). That suggests that for a consideration of the proximity to the cut-off frequency relations (4.4) should be consulted, rather than the non-dimensional counterparts given by (B.3).

The imaginary part of the wave number is a measure of penetration depth of the evanescent waves in the axial direction of the plate. Some authors consider the smallest K to be a measure for validity of the dynamical version of Saint-Venant's principle, in analogy with the decay rate in the quasi-static case of plate problems (Torvik, 1967; Karp and Durban, 1997). Evanescent waves are also related to the phenomenon of energy trapping either at the edge of a waveguide or, at any discontinuity within or along the generators of the waveguide (e.g., Linton et al., 2002). Thus, denoting complex wave numbers by

$$k = J + \mathrm{i}K \quad \text{with } K > 0 \tag{4.6}$$

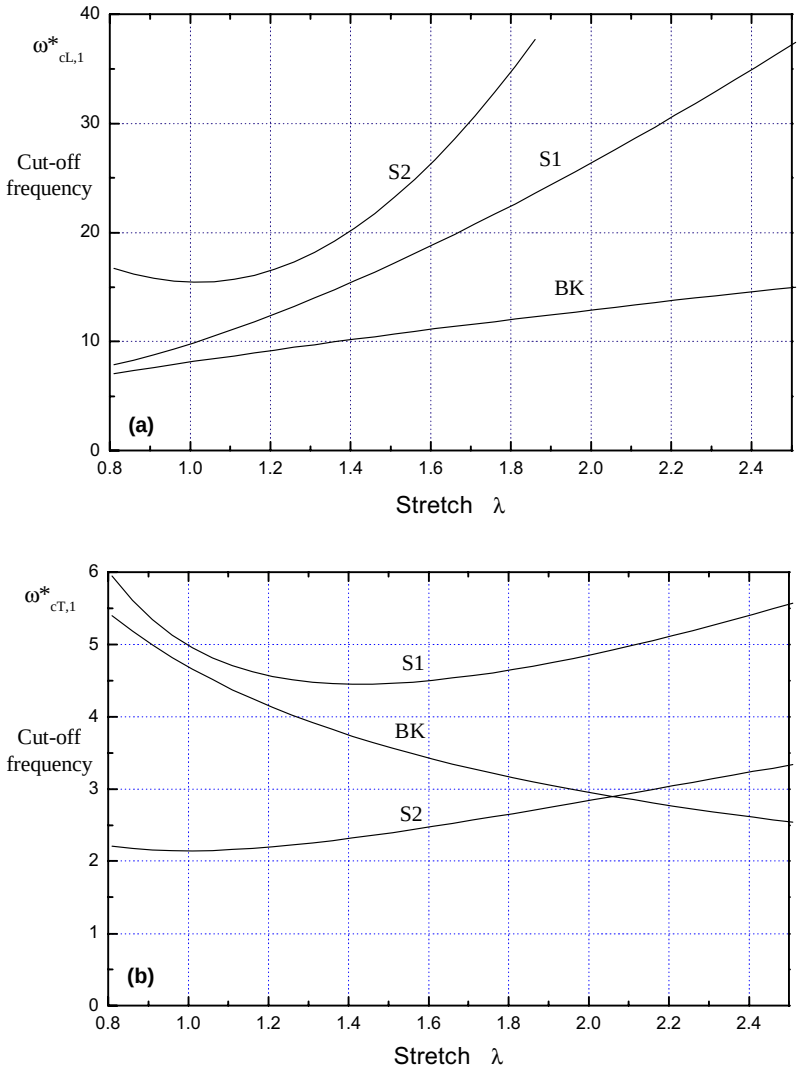

Fig. 16. First cut-off reference (physical) frequencies for the three materials. Dimensions of physical frequencies are in $\sqrt{N}/\text{mm}$: (a) first longitudinal cut-off frequency; (b) first transverse cut-off frequency.

we may argue, in the spirit of elastostatics, that the smallest value of the attenuation constant K provides a bound on axial attenuation, of dynamic harmonic perturbation, inversely related to the depth of penetration of that mode. The relevance of that attenuation in the presence of propagating modes in a dynamic problem is detailed in Karp and Durban (1997).

A general observation, based on the frequency maps and relation (3.4) is that at frequencies just below any cut-off frequency, a small value of K is possible-implying a large distance of penetration of the evanescent mode.

Fig. 17 displays the variation of the smallest attenuation constant $K_{\min}$ with initial stretch for the BK material at several reference frequencies. Similar results are shown in Fig. 18 (S1 with sliding boundaries). These figures reveal a rich and complex picture, with considerable sensitivity of $K_{\min}$ to initial stretch,

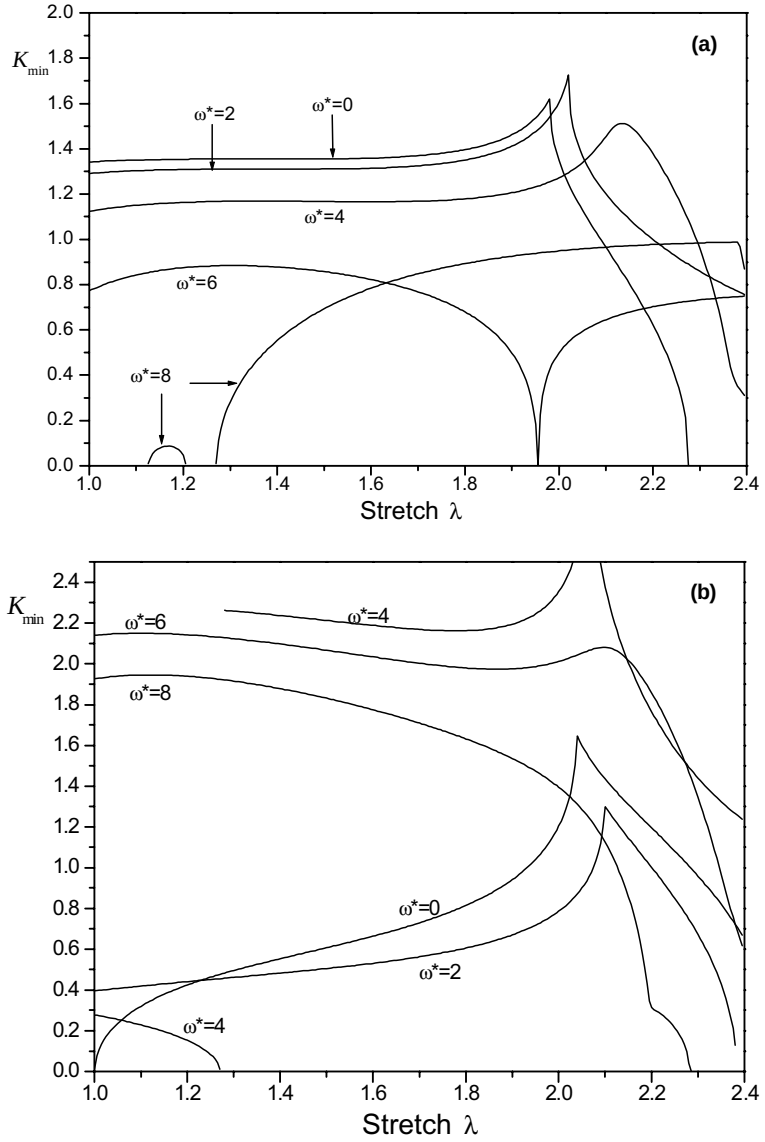

Fig. 17. Variation of the smallest attenuation constant $K_{\min}$ with initial stretch. BK material with free boundaries. Values of physical reference frequency are indicated in the figure with dimensions of $\sqrt{N}/\text{mm}$. (a) Symmetric modes, (b) antisymmetric modes.

frequency, and boundary data and are typical to other boundary conditions (as can be judged from Figs. 2–15).

We do not discuss here the question of quasi-static bifurcation of the background finite deformation and the properties of propagating modes, studied extensively by Roxburgh and Ogden (1994) and in recent works by Rogerson et al. Nevertheless, a few comments related to propagating waves deserve notice.

Semi-infinite plates with free boundaries will buckle at a vanishingly small compressive load. With small initial stretch, $\lambda = 1 + \Delta$ where $|\Delta| \ll 1$, we have from (3.12) the approximation, again for the BK material ($\nu_0 = 1/4$),

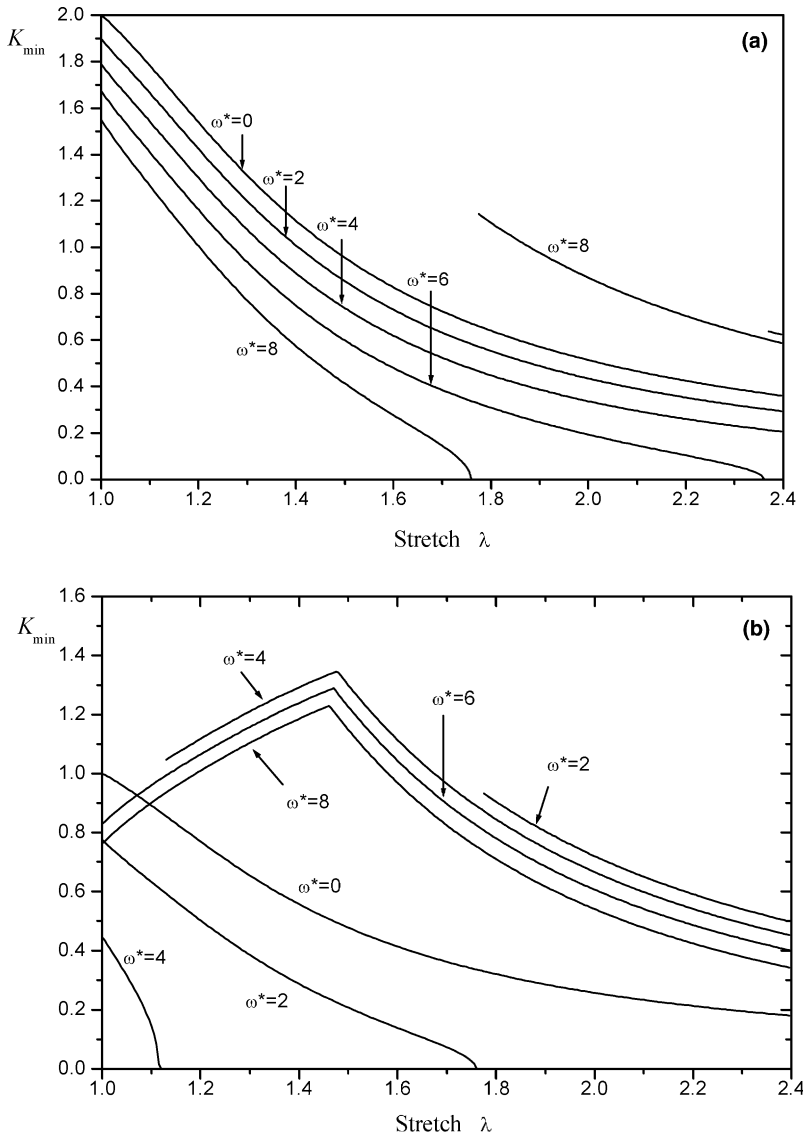

Fig. 18. Variation of the smallest attenuation constant $K_{\min}$ with initial stretch. S1 material with sliding boundaries. Nomenclature as in Fig. 17. (a) Symmetric modes, (b) antisymmetric modes.

$$k = \frac{\sqrt{3}}{2\sqrt{2}} \frac{\Omega}{\sqrt{\Delta}} \tag{4.7}$$

which, in fact, is valid also for negative values of Δ. At the stress free configuration relation (4.7) is replaced by

$$k^2 = \pm \frac{3}{\sqrt{2}\pi} \Omega \tag{4.8}$$

Fig. 19a shows the details of frequency maps (BK, free boundaries, antisymmetric modes) at, and near, the stress free configuration, both in compression ($\lambda = 0.8$) and tension ($\lambda = 1.1$). The validity of (4.7) and (4.8)

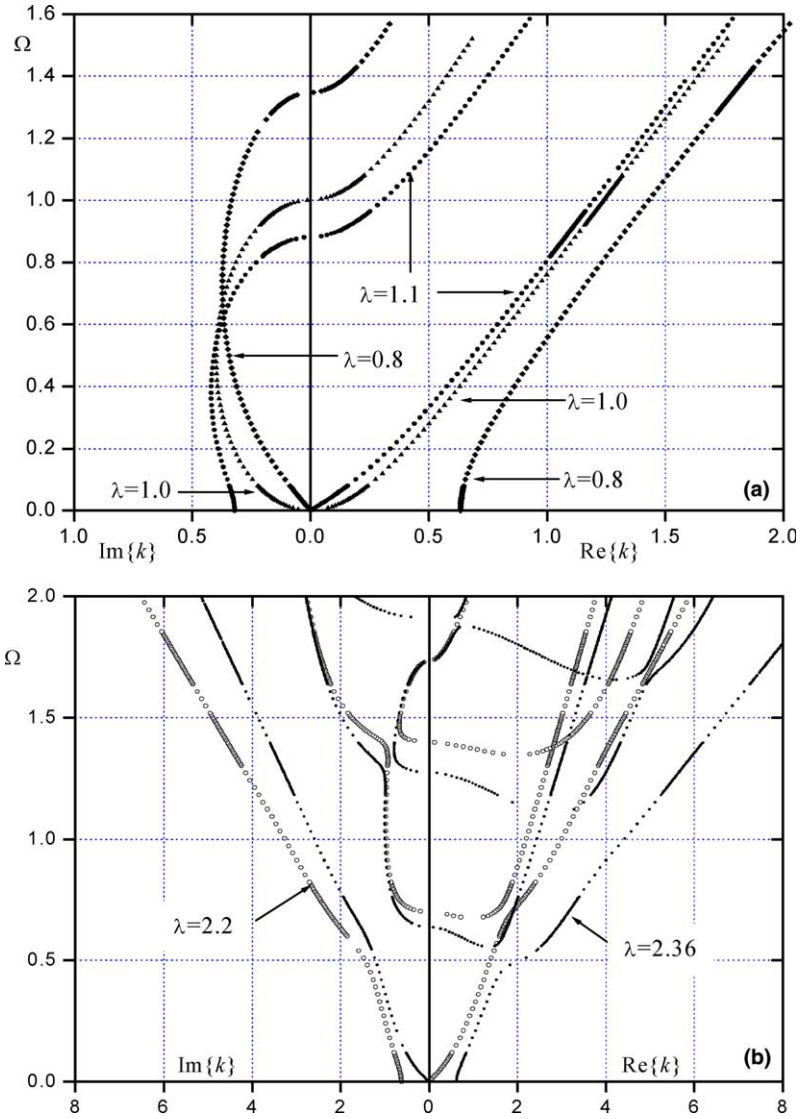

Fig. 19. Frequency maps for the BK material with free boundaries in the vicinity of bifurcation states. (a) Antisymmetric modes near the stress free state. (b) Symmetric modes near necking.

near the origin is clearly seen. These results are also confirmed for the static case ($\Omega = 0$) by comparison with the asymptotic result derived by Durban and Karp (1992)

$$k = \frac{2\sqrt{3}}{\pi} i\sqrt{\Delta} \quad \text{for } \Omega = 0 \tag{4.9}$$

All three relations (4.7)–(4.9) indicate low decay rates (large depth of penetration of edge disturbances) near the stress free configuration. A recent study on decay of end effects in elastostatics, with initial compression, has been given by Karp (in press).

Finally, in Fig. 19b we examine the symmetric modes at stretches slightly below ($\lambda = 2.2$), and slightly above ($\lambda = 2.36$), the necking stretch ($\lambda = \lambda_u \approx 2.28$) of the BK material with free boundaries. Relation (3.7), along with its static analogue (Durban and Karp, 1992)

$$k = \frac{6\sqrt{3}}{\pi} \mathrm{i} \sqrt{1 - \frac{\lambda}{\lambda_u}} \quad \text{for } \Omega = 0 \tag{4.10}$$

are in complete agreement with numerical calculations. It is interesting to note that for both post-bifurcated states in Fig. 19a and b ($\lambda = 0.8$ and 2.36) the propagating mode originates at the $\Omega = 0$ line and is characterized by vanishing phase velocity and an infinite group velocity.

The traction rate resultants produced by the eigenmodes, at the disturbed end $z = 0$, are generally not self-equilibrated. Of course, for symmetric modes no resultant shear traction rate (F_x) or resultant moment rate (M) will develop at the loaded end. However, the axial traction rate becomes

$$F_z = \frac{\frac{2h\mathrm{i}}{\pi} bk[\![T_{xz}]\!] - \beta c \Omega^2 [\![U]\!]}{bk^2 - \beta \Omega^2} \mathrm{e}^{-\mathrm{i}\omega t} \tag{4.11}$$

where T_{xz} denotes the transverse profile of the shear traction rate defined in (2.8) as $(\overset{\nabla}{\tau}_{xz} - \sigma\gamma_{xz})$, and $[\![\cdot]\!]$ stands for through thickness jumps, for example

$$[\![U]\!] \equiv U(h) - U(-h) \tag{4.12}$$

Relation (4.11) follows directly from the equations of motion, and from the constitutive relations, and is not restricted to symmetric modes. For free boundaries, where T_{xz} vanishes at $x = \pm h$, F_z remains active unless $\Omega = 0$ (quasi-static response). Exceptionally, for sliding boundaries, where both T_{xz} and U vanish at $x = \pm h$, F_z vanishes as well and each eigenmodes is fully self-equilibrating.

The analogous expressions for the resultant shear traction rate and for the resultant moment rate are readily found as

$$F_x = \frac{\frac{2h\mathrm{i}}{\pi} k[\![T_{xx}]\!] - \alpha \Omega^2 [\![W]\!]}{k^2 - \Omega^2} \mathrm{e}^{-\mathrm{i}\omega t} \tag{4.13}$$

$$M = -\frac{\frac{2h\mathrm{i}}{\pi} bk(F_x - [\![xT_{xz}]\!]) + \frac{2h\mathrm{i}}{\pi}(c - \sigma)\left(kF_x - \frac{2h\mathrm{i}}{\pi}[\![T_{xx}]\!]\right) + \beta c \Omega^2 [\![xU]\!]}{bk^2 - \beta \Omega^2} \mathrm{e}^{-\mathrm{i}\omega t} \tag{4.14}$$

where T_{xx} denotes the transverse profile of the normal traction rate defined in (2.8) as $\overset{\nabla}{\sigma}_x$.

Both F_z and M will vanish for any symmetric wave and in the static case for antisymmetric modes when the boundaries are free. For inextensional waves, F_z will vanish at any frequency, but otherwise, self-equilibrium of the eigenmodes is not maintained. In fact, for free and clamped boundaries it is possible to relate the traction rate resultants, (4.11) and (4.13), to averaged end velocities U_{av} and W_{av} by the elegant formulae

$$F_x = \mathrm{i}\pi \frac{\beta}{k} \Omega^2 U_{av}, \quad F_z = \mathrm{i}\pi \frac{\beta}{k} \Omega^2 W_{av} \tag{4.15}$$

for free boundaries, and

$$F_x = \mathrm{i}\pi k \beta U_{av}, \quad F_z = \mathrm{i}\pi k b W_{av} \tag{4.16}$$

for clamped boundaries. These relations can be used to examine the influence of Ω on the instantaneous impedance.

While most of existing studies concentrate on the phase velocity of the propagating waves we draw attention to the group velocity which is related to energy propagation. Such disposition exposes interesting

implications of the frequency analysis. For example, according to (3.4) the group velocity of waves at frequencies just above a cut-off frequency is very small, thus having negligible contribution to energy propagation albeit a very large phase velocity. Another example is the flexural mode in a plate with free faces. According to (3.10), the group velocity of that mode in a stress free state is very small at low frequencies. Application of even incremental prestress to the plate dictates wave propagation according to (3.9) which induces finite group velocity even at a very low frequency. Considering the plate's own weight as generating small prestress raises the question of the possibility to experimentally observe the behaviour predicted by linear elasticity (3.10) in working structures (though observed in a careful experiments carried by Zemanek, 1972). That observation is consistent with the known result for a vibrating string which will not vibrate unless initial tension T is applied, resulting in the phase velocity $C = \sqrt{T/\rho}$ (see also discussion by Kaplunov et al., 2000).

5. Concluding comments

We have presented a detailed spectral analysis of dynamic eigenfields generated, within a prestrained plate, by time harmonic end excitation. Exact equations of non-linear continuum elasticity have been used, in a rate version, to obtain closed-form separation of variables solutions. Frequency maps are provided over a range of excitation frequency and prestrain, with several sets of boundary conditions, and for three different hyperelastic materials, and compared to the corresponding frequency maps obtained for a stress free plate (representing the solution of linear elasticity).

Depth of penetration of evanescent modes, related to trapped energy, is discussed. In particular, a large depth of penetration in the proximity to the cut-off frequencies is observed along with cut-off frequency sensitivity to the prestretch. It has been noted that caution should be practised while considering proximity to cut-off frequencies in terms of non-dimensional frequencies. High sensitivity of the maximal possible depth of penetration to initial stretch, with abrupt changes due to crossings of cut-off frequencies, is exposed. Two typical cases are shown graphically.

The four ideal symmetric cases of boundary conditions have been discussed along with a few non-symmetric combinations of boundary data. It is expected that such cases might be relevant to waveguides with partial or non-symmetric coating (like electroplating, e.g. Johnson et al., 1996). The eigenfield investigated here are of particular interest in the analysis of dynamic response of finite plates, with various boundary conditions, as they enable a spectral expansion in the eigenmodes. The similarity of the frequency maps for plates with both faces free of traction to plates with both faces clamped are noticed. Plates with inextensional and sliding faces possess identical frequency maps, except for exchange of symmetric with antisymmetric modes and the existence of only one fundamental mode in each case.

The traction rate resultants, related to acoustic impedance, are derived, and expressed in terms of boundary data over the long faces. In general, self-equilibrium of the waves is not maintained. While self-equilibrium is an important notion in static analysis of Saint-Venant's principle, that finding in dynamics does not necessarily excludes the possibility of existence of a dynamic version of Saint-Venant's principle (e.g., Karp and Durban, 1997).

Acknowledgments

Part of this study was supported by the fund for the promotion of research at the Technion. D.D. is grateful for the kind assistance of the Sydney Goldstein Chair in Aeronautical Engineering.

Appendix A. Instantaneous moduli for hyperelastic solids

Hyperelastic isotropic solids admit a strain energy function of the form $W(\lambda_x, \lambda_y, \lambda_z)$ with the plane strain moduli (Hill, 1978)

$$a \equiv \frac{\lambda_x}{\lambda_z}\frac{\partial^2 W}{\partial \lambda_x^2}, \quad b \equiv \frac{\lambda_z}{\lambda_x}\frac{\partial^2 W}{\partial \lambda_z^2}, \quad c \equiv \frac{\partial^2 W}{\partial \lambda_x \partial \lambda_z}, \quad 2\mu \equiv \frac{\lambda_x^2 + \lambda_z^2}{\lambda_x^2 - \lambda_z^2}(\sigma_x - \sigma_z) \tag{A.1}$$

In this study we consider the hyperelastic family (Hill, 1978)

$$W = \sum_j \frac{C_j}{m_j}\left[\lambda_1^{m_j} + \lambda_2^{m_j} + \lambda_3^{m_j} - 3 + \frac{1}{n}(J^{-nm_j} - 1)\right] \tag{A.2}$$

where the principal stretches $(\lambda_1, \lambda_2, \lambda_3)$ are identified as $\lambda_1 = \lambda_z = \lambda$, $\lambda_2 = \lambda_y = 1$, $\lambda_3 = \lambda_x = \lambda^{-n/(n+1)}$ and $J = \lambda_1\lambda_2\lambda_3$ is the volume ratio. The summation is carried over pairs (C_j, m_j) which, like n, are experimentally determined material parameters.

The instantaneous moduli (A.1) follow in the form (Durban and Karp, 1992)

$$a = (n+1)\sum_j C_j m_j \lambda^{-\frac{nm_j+1}{n+1}} \tag{A.3a}$$

$$b = \sum_j C_j\left[(m_j - 1)\lambda^{\frac{(n+1)m_j-1}{n+1}} + (nm_j + 1)\lambda^{-\frac{nm_j+1}{n+1}}\right] \tag{A.3b}$$

$$c = n\sum_j C_j m_j \lambda^{-\frac{nm_j+1}{n+1}} \tag{A.3c}$$

$$2\mu = \frac{\lambda^{\frac{2(2n+1)}{n+1}} + 1}{\lambda^{\frac{2(2n+1)}{n+1}} - 1}\sigma \tag{A.3d}$$

where $\sigma \equiv \sigma_z$ is given by the (plane-strain) stress–stretch relation

$$\sigma = \lambda^{-\frac{1}{n+1}}\sum_j C_j\left(\lambda^{m_j} - \lambda^{-\frac{nm_j}{n+1}}\right) \tag{A.4}$$

The three specific models used in the numerical evaluation of the eigenvalues are the Blatz–Ko foam rubber (Blatz and Ko, 1962) with the single term representation

$$\text{(BK)} \quad m_1 = -2, \quad C_1 = -22, \quad n = 0.5 \qquad (\nu_0 = 0.25) \tag{A.5}$$

and two vulcanized foam rubbers due to Storåkers (1986): a highly compressible natural rubber (S1) with

$$\text{(S1)} \quad m_1 = -m_2 = 4.5, \quad C_1 = 1.85, \quad C_2 = -9.2, \quad n = 0.92 \qquad (\nu_0 = 0.324) \tag{A.6}$$

and a nearly incompressible synthetic rubber (S2) with

$$\text{(S2)} \quad m_1 = -m_2 = 3.6, \quad C_1 = 2.04, \quad C_2 = -0.51, \quad n = 25 \qquad (\nu_0 = 0.49) \tag{A.7}$$

Here the dimensions of parameters C_j in that data are $10^{-2}\,\mathrm{N\,mm^{-2}}$.

In the absence of prestrain ($\lambda = 1$) we recover from (A.3a–d) the usual elastic moduli, of the stress free configuration,

$$2\mu_0 = \sum_i m_i C_i, \quad \nu_0 = \frac{n}{2n+1}, \quad a = b = 2(n+1)\mu_0, \quad c = 2n\mu_0, \quad \alpha = \beta = \mu_0 \tag{A.8}$$

where μ_0 is the shear modulus and ν_0 is the Poisson ratio.

For the Blatz–Ko material (A.5) the instantaneous moduli (A.3) admit the simple form

$$a = 3\mu_0, \quad b = 3\mu_0 R, \quad c = \mu_0, \quad \alpha = \mu_0 R, \quad \beta = \mu_0 \tag{A.9}$$

where

$$R \equiv \lambda^{-8/3} \tag{A.10}$$

Likewise, the instantaneous shear modulus and the stress-strain relation (under plane-strain constraint) are given by

$$2\mu = \mu_0(1+R), \quad \sigma = \mu_0(1-R) \tag{A.11}$$

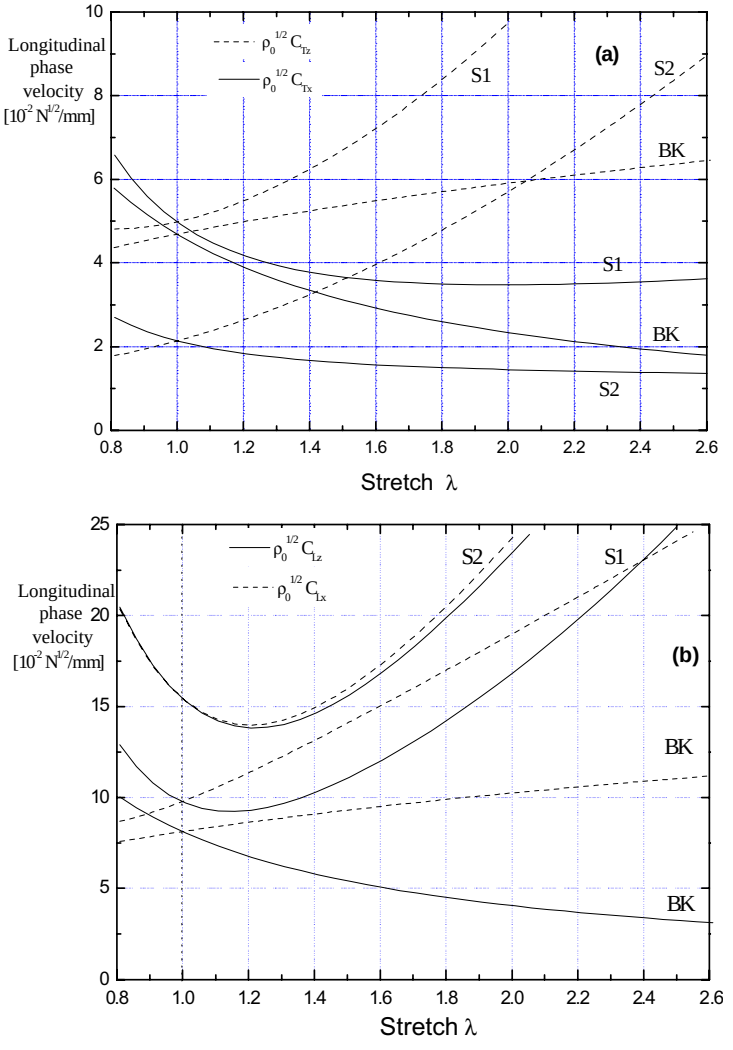

Fig. A.1. Variation of reference phase velocities with initial stretch for three hyperelastic materials: (a) transverse velocities, (b) longitudinal velocities.

Fig. 1 shows the force ($F = \lambda_x \sigma$) required to produce the (plane-strain) stretch λ for each of the three solids (A.5)–(A.7). It is seen that the BK material has a necking instability at the stretch $\lambda_u \approx 2.28$ where F attains its highest value (Durban and Karp, 1992).

The reference phase velocities (2.7) vary with initial stretch, and can be conveniently rewritten as

$$\sqrt{\rho_0} C_{Tx} = \sqrt{J\alpha}, \quad \sqrt{\rho_0} C_{Tz} = \sqrt{J\beta}, \quad \sqrt{\rho_0} C_{Lx} = \sqrt{Ja}, \quad \sqrt{\rho_0} C_{Lz} = \sqrt{Jb} \tag{A.12}$$

where ρ_0 is the background density of the undeformed state, and

$$J = \frac{\rho_0}{\rho} = \lambda^{\frac{1}{n+1}} \tag{A.13}$$

Relations (A.12) are displayed in Fig. A.1 for the three materials considered here. Initially, with $\lambda = 1$, there are just two different velocities, since $\alpha = \beta = \mu_0$ and $a = b = 2(n+1)\mu_0$ imply that $C_{Tx} = C_{Tz}$ and $C_{Lx} = C_{Lz}$. As the deformation progresses, however, all four velocities are, in general, activated with considerable sensitivity to the stretch λ.

For the BK solid (A.9) and (A.10) we find that the phase velocities can be easily related to the axial stretch by

$$\sqrt{\rho_0} C_{Tx} = \sqrt{\mu_0}\lambda^{-1}, \quad \sqrt{\rho_0} C_{Tz} = \sqrt{\mu_0}\lambda^{1/3}, \quad \sqrt{\rho_0} C_{Lx} = \sqrt{3\mu_0}\lambda^{1/3}, \quad \sqrt{\rho_0} C_{Lz} = \sqrt{3\mu_0}\lambda^{-1} \tag{A.14}$$

Appendix B. Cut-off frequencies

Cut-off frequencies are obtained at the limit of vanishing wave numbers, $k \to 0$, rendering the incremental displacements (2.13) independent of the axial coordinate. The time harmonic solutions of the equations of motion (2.4) and (2.5) are then given by the reduced version of (2.13), for $k = 0$, with

$$U_s = A \sin\left(\sqrt{\frac{\rho}{a}}\omega x\right), \quad W_s = B \cos\left(\sqrt{\frac{\rho}{\alpha}}\omega x\right) \tag{B.1}$$

$$U_a = C \cos\left(\sqrt{\frac{\rho}{a}}\omega x\right), \quad W_a = D \sin\left(\sqrt{\frac{\rho}{\alpha}}\omega x\right) \tag{B.2}$$

Compliance with the boundary data (2.23)–(2.26) generates, in all cases, two groups of cut-off frequencies given by multiples of the reference velocities C_{Lx} and C_{Tx} of 2.7. Thus, with the non-dimensionalization of (2.19) the cut-off frequencies are

$$\Omega_{CL} = m\frac{C_{Lx}}{C_{Tz}} = m\sqrt{\frac{a}{\beta}}, \quad \Omega_{CT} = n\frac{C_{Tx}}{C_{Tz}} = n\sqrt{\frac{\alpha}{\beta}}, \quad m, n = 1, 2, 3, \ldots \tag{B.3}$$

with integers (m,n) labeling longitudinal and transverse waves, respectively. Fig. B.1 displays the dependence of the first ($m = 1$, $n = 1$) cut-off frequencies on initial stretch for the three hyperelastic solids considered here.

For the BK material we have, with the aid of (A.9) and (A.10),

$$\Omega_{CL} = \sqrt{3}m, \quad \Omega_{CT} = \lambda^{-4/3}n, \qquad m, n = 1, 2, 3, \ldots \tag{B.4}$$

At the stress free configuration we recover from (B.3) the known relations, using (A.8),

$$\Omega_{CL} = m\sqrt{2(n+1)} = m\sqrt{\frac{2(1-\nu_0)}{1-2\nu_0}}, \quad \Omega_{CT} = n. \tag{B.5}$$

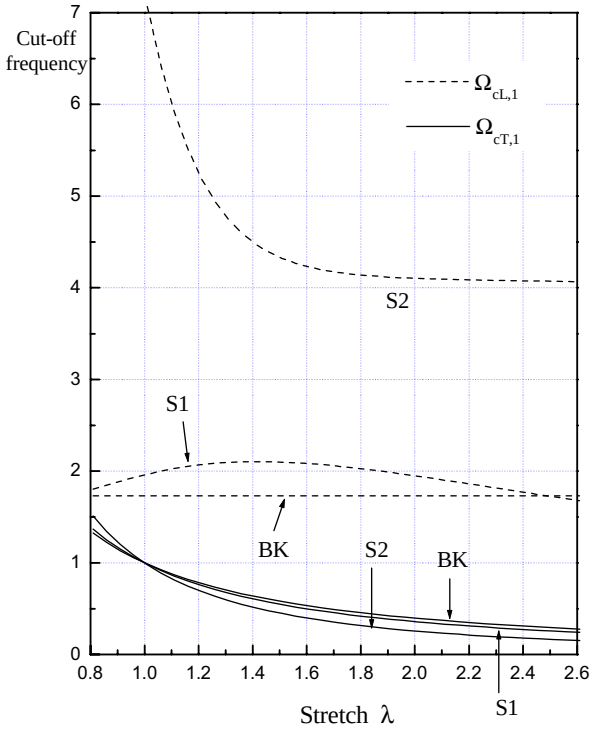

Fig. B.1. Variation of cut-off frequencies with initial stretch for three hyperelastic materials. Curves are for the first frequencies of (B.3), with $m = 1$ and $n = 1$. Higher frequencies are obtained as simple multiples of the first frequencies.

Here, the n letter under the square root sign in the expression for Ω_{CL} is the material property as used in (A.2) and indicating, as expected, that for nearly incompressible material the thickness-stretch cut-off frequency approaches infinity.

References

Achenbach, J.D., 1973. Wave Propagation in Elastic Solids. North-Holland, Amsterdam.

Blatz, P.J., Ko, W.L., 1962. Application of finite elastic theory to the deformation of rubbery materials. Trans. Soc. Rheo. 6, 223–251.

Chadwick, P., Jarvis, D.A., 1979. Surface waves in a pre-stressed elastic body. Proch. R. Soc. Lond. A 366, 517–536.

Durban, D., Karp, B., 1992. Axial decay of self-equilibrating end loads in compressible solids. J. Appl. Mech.—Trans. ASME 59, 738–743.

Hill, R., 1978. Aspects of invariance in solid mechanics. Adv. Appl. Mech. 18, 1–75.

Hill, R., 1979. On the theory of plane strain in finitely deformed compressible materials. Math. Proc. Camb. Phil. Soc. 86, 161–178.

Horgan, C.O., Knowles, J.K., 1983. Recent developments concerning Saint-Venant's principle. Adv. Appl. Mech. 23, 179–269.

Johnson, G.C., Chen, S.-E., 1989. The influence of applied stress on the response of thin films. In: McCarthy, M.F., Hayes, M.A. (Eds.), Elastic Wave Propagation. Elsevier, Amsterdam.

Johnson, W., Auld, B.A., Segal, E., Passarelli, F., 1996. Trapped torsional modes in solid cylinders. J. Acoust. Soc. Am. 100, 285–293.

Kaplunov, J.D., 1995. Long-wave vibrations of a thin-walled body with fixed faces. Q. J. Mech. Appl. Math. 48, 311–327.

Kaplunov, J.D., Nolde, E.V., 2002. Long-wave vibrations of nearly incompressible isotropic plate with fixed faces. Q. J. Mech. Appl. Math. 55, 345–356.

Kaplunov, J.D., Nolde, E.V., Rogerson, G.A., 2000. A low-frequency model for dynamic motion in pre-stressed incompressible elastic structures. Proc. R. Soc. Lond. A 456, 2589–2610.

Kaplunov, J.D., Nolde, E.V., Rogerson, G.A., 2002. Short wave motion in a pre-stressed incompressible elastic plate. IMA J. Appl. Math. 67, 383–399.

Karp, B., 1996. On Saint-Venant's Principle in Elastostatics and Elastodynamics, D.Sc. Thesis, Technion, Haifa.

Karp, B., in press. End effects in prestrained plates under compression. J. Appl. Mech.—Trans. ASME.

Karp, B., Durban, D., 1997. Towards a dynamic version of Saint-Venant's principle. In: Gilchrist, M.D. (Ed.), Modern Practice in Stress and Vibration analysis, 3rd International Conference, Dublin, Ireland, 3–5 September 1997. A.A. Balkema, Rotterdam, ISBN 90 5410 896 7.

Karp, B., Durban, D., 2002. Influence of boundary conditions on decay rates in a prestrained plate. J. Appl. Mech.—Trans. ASME 69, 515–520.

Linton, C.M., McIver, M., McIver, P., Ratcliffe, K., Zhang, J., 2002. Trapped modes for off-centre structures in guides. Wave Motion 36, 67–85.

McCoy, J.J., 1968. Effects of non-propagating plate waves on dynamical stress concentrations. Int. J. Solids Struct. 4, 355–370.

Mindlin, R.D., 1960. Waves and vibrations in isotropic elastic plates. In: Goodier, J.N., Hoff, N.J. (Eds.), Structural Mechanics. Pergamon, New York.

Nolde, E.V., Rogerson, G.A., 2002. Long wave asymptotic integration of the governing equations for a pre-stressed incompressible elastic layer with fixed faces. Wave Motion 36, 287–304.

Ogden, R.W., Roxburgh, D.G., 1993. The effect of pre-stress on the vibration and stability of elastic plates. Int. J. Engng. Sci. 31, 1611–1636.

Pichugin, A.V., Rogerson, G.A., 2001. A two-dimensional model for the extensional motion of a pre-stressed incompressible elastic layer near cut-off frequencies. IMA J. Appl. Math. 66, 357–385.

Press, W.H., Flannery, B.P., Teukolsky, S.A., Vetterling, W.T., 2001. The Numerical Recipes in FORTRAN: the Art of Scientific Computing, second ed. Cambridge University Press, Cambridge.

Rogerson, G.A., 1997. Some asymptotic expansions of the dispersion relation for an incompressible elastic plate. Int. J. Solids Struct. 34, 2785–2802.

Rogerson, G.A., Cai, Z., 2000. Infinitesimal harmonic wave propagation in a homogeneously pre-strained idealized fibre-reinforced layer. ZAMP 51, 591–610.

Roxburgh, D.G., Ogden, R.W., 1994. Stability and vibration of pre-stressed compressible elastic plates. Int. J. Engng. Sci. 32, 427–454.

Storåkers, B., 1986. On material representation and constitutive branching in finite compressible elasticity. J. Mech. Phys. Solids 34, 125–145.

Torvik, P.J., 1967. Reflection of wave trains in semi-infinite plates. J. Acoust. Soc. Am. 41, 346–353.

Zemanek Jr., J., 1972. An experimental and theoretical investigation of elastic wave propagation in a cylinder. J. Acoust. Soc. Am. 51, 265–283.